



Article

Silicates from Lherzolites in the South-Eastern Part of the Kempirsay Massif as the Source for Giant Chromitite Deposits (the Southern Urals, Kazakhstan)

Dmitri E. Saveliev ¹, Darkhan K. Makatov ², Ildar R. Rakhimov ^{1,*} , Ruslan A. Gataullin ¹ and Vladimir V. Shilovskikh ³ 

¹ Ufa Federal Research Center, Institute of Geology, Russian Academy of Sciences, 16/2 Karl Marx Street, 450077 Ufa, Russia

² The Department of Geology and Exploration of Mineral Deposits, Karaganda Technical University, 56 Nursultan Nazarbaev Avenue, Karaganda 100027, Kazakhstan

³ Geomodel Center, Saint-Peterburg University, 20 Parkovaya Street, Peterhoff, 198504 Saint-Petersburg, Russia

* Correspondence: rigel92@mail.ru



Citation: Saveliev, D.E.; Makatov, D.K.; Rakhimov, I.R.; Gataullin, R.A.; Shilovskikh, V.V. Silicates from Lherzolites in the South-Eastern Part of the Kempirsay Massif as the Source for Giant Chromitite Deposits (the Southern Urals, Kazakhstan). *Minerals* **2022**, *12*, 1061. <https://doi.org/10.3390/min12081061>

Academic Editors: Jingsui Yang, Souvik Das and Weiwei Wu

Received: 22 July 2022

Accepted: 20 August 2022

Published: 22 August 2022

Publisher's Note: MDPI stays neutral with regard to jurisdictional claims in published maps and institutional affiliations.



Copyright: © 2022 by the authors. Licensee MDPI, Basel, Switzerland. This article is an open access article distributed under the terms and conditions of the Creative Commons Attribution (CC BY) license (<https://creativecommons.org/licenses/by/4.0/>).

Abstract: We provide results of a comprehensive mineralogical and microstructural study of relict lherzolites of the main ore field and fresh rocks from a deep structural borehole drilled in the south-eastern part of the Kempirsay massif. Olivine and orthopyroxene from lherzolites contain numerous pieces of evidence of material redistribution at different scales caused mainly by solid-state processes, such as plastic flow of mantle, syntectonic recrystallization, and annealing. The results of deformation-induced processes at the submicron scale are recorded by optical and electronic microscopy. In olivine, the plastic deformation caused segregation of impurities at structural defects. As a result, abundant tiny rods of newly formed Cr-spinels occurred inside its grains. Moreover, in enstatite, deformation caused partial or complete chemical decomposition with exsolution of diopside, pargasite and spinel lamellae up to the formation of a “fibrous” structure. In other cases, it provided partial or complete recrystallization to form new phases of enstatite-2, forsterite, diopside, pargasite, and spinel. Petrographic observations are validated by geochemical data, i.e., regularly decreasing concentrations of minor elements in neoblasts compared to large grains (porphyroclasts). Further redistribution of spinel grains with the formation of chromitite bodies is witnessed by their permanent association with the most mobile phase of the upper mantle, i.e., olivine, which is the only mineral that remains stable under the intense plastic flow. An increased concentration of Cr-spinel grains during formation of massive chromitites could appear under conditions close to pressure sintering, as evidenced by stressed textures of ores and an increased grain size compared to disseminated chromitites. The formation of unique chromitite deposits is associated with integration of numerous disparate podiform bodies into “ore bunches” due to the tectonic impact in the shear-compression regime. This was most likely associated with transition of the rifting (spreading) regime to that of the upper mantle of the fore-arc basin.

Keywords: peridotite; enstatite; olivine; Cr-spinel; plastic deformation; chromitite; Kempirsay; South Urals; Kazakhstan

1. Introduction

The problem of formation of chromitite bodies in the mantle section of ophiolite complexes is far from being solved. This is evidenced by numerous publications on this topic that offer various interpretations of dunite-chromitite assemblages. Different versions of the reactive hypothesis introduced by P. Kelemen [1] are most commonly used for explanation. Notably, compositions of interaction melts are the most typical study object [2–5], although the mechanism of concentration of Cr-spinel grains as ore bodies is substantiated in this model insufficiently.

At the same time, an increasing number of works inferring the leading role of fluids and hydrothermal processes in ore genesis from the study of mineral inclusions in chromite grains [6–9]. In addition to the absence of a concentration mechanism, another crucial problem of the mentioned hypotheses is that chromitites are always enclosed in dunite envelopes with no traces of melts or fluids, not counting microinclusions of hydrous silicates (pargasite, phlogopite, etc.) in Cr-spinel grains.

In previous studies, on the example of the Kraka and Nurali ultramafic rocks, we showed that new grains of Cr-spinel could be formed during segregation of impurities and deformation-induced decomposition of enstatite and olivine [10,11]. At the same time, similar segregations of minerals non-typical for ultramafic rocks are often found together with thin Cr-spinel precipitations. The observed facts became an essential part of the model of rheomorphic differentiation of material in the ascending mantle diapirs [12]. This model suggests formation of new portions of Cr-spinel grains with a simultaneous decrease in the amount of pyroxenes (peridotite-dunite transition) and further segregation of grains in the plastic flow. A similar mechanism of chromite concentration in result of intensive plastic deformation was proposed for deposits in the Xerolivado region [13].

The productivity of this process is one of our opponents' questions to the model, since there are no major chromitite deposits in the earlier studied massifs. In this paper, we consider lherzolites of the Kempirsay massif with the unique chromite content that display the same microstructural features indicating solid-state mechanisms of material redistribution in the upper mantle.

The Kempirsay massif has been studied for several decades by a set of methods, geophysical, mineralogical, geochemical ones inclusive; it was also investigated at the depth by comprehensive structural and exploratory drilling [14–17], etc. Early works of Soviet researchers suggested two major viewpoints on the genesis of ultramafic rocks and associated chromitite, i.e., igneous and metasomatic. As for the former one, ultramafic rocks were considered derivatives of ultramafic melt that entered the geosynclinal stage of the Uralian Mobile Belt evolution along a deep fault [15,18], while chromitites were formed as magmatic differentiates or liquation products [14]. In the latter version, great importance was attached to the tectonic redistribution of ores within the dunite-harzburgite association. According to the metasomatic hypothesis (Moskaleva 1974), dunites and chromitites were formed by transformation of primary enstatites during olivinization under the influence of magnesian fluids.

It is now generally accepted that peridotites in the ophiolite mantle section are restites from partial melting of the upper mantle material (e.g., [19,20]), but the role of magmatic and metasomatic processes in formation of dunites and chromitites is still debated (e.g., [1,21–23]). Recent decades were marked by several papers on geodynamic settings for the ultramafic rock formation in the Kempirsay massif [24–26], the genesis of chromitites [16,25,27] and associated accessory mineralization [28,29].

Most of the mentioned works consider ultramafic rocks of the Kempirsay massif as restites from partial melting of the fertile lherzolites in the upper mantle of the Uralian paleo-ocean. The formation of dunites and chromitites is associated either with percolation through restite harzburgites of melts similar to boninites in supra-subduction settings [24,25,27], or with the fluid-metasomatic impact of reduced fluids on ultramafic rocks [16,26]. Our data generally comply with earlier studies, though, as shown below, we provide a slightly different interpretation of both the geodynamic history of the massif and the mechanism of chromium concentration and position of chromitite bodies in dunites.

2. Geological Setting

The Kempirsay ultramafic massif is one of the largest in the Urals, covering an area of more than 1000 km². The massif is located in the southern part of the fold belt, at the junction of two paleobasins, the Sakmar (Sakmar zone) and the Magnitogorsk-Mugodzhzar (Magnitogorsk megazone). In the northern part, it is separated from the Magnitogorsk megazone by the Ebeta zone of metamorphic rocks, which is the southern continuation

of the Uraltau zone (Figure 1). The central part of the massif is composed of dominant harzburgites with subordinate lherzolites and dunites. In the south-eastern part, the amount of dunites increases and the so-called dunite-harzburgite unit is mapped, where the proportion of dunites varies from 10% to 60% (e.g., [14]). On the surface, ultramafic rocks were generally subject to low-temperature mesh serpentinization and significant weathering. Rocks with relics of primary mantle minerals are very rare, usually only accessory Cr-spinel is preserved in the rocks. With depth, the proportion of serpentine decreases, which allows studying the composition and structure of primary mantle minerals in core samples from exploration and deep structural boreholes.

Country rocks occur as volcanic-sedimentary sequences of the Sugralinskaya suite (basalts, tuffs, siliceous sediments), usually comparable with the upper crust sections of ophiolites. Volcanic rocks are represented by effusive facies of tholeiite pillow basalts; their composition is similar to MOR tholeiites [30,31]. Mafic rocks are widespread along the frame of ultramafic rocks. They are subdivided into several units, i.e., the Kokpekta layered gabbroid unit, Shandasha isotropic gabbro-diorite unit and Kyzylkain pyroxenite-gabbro unit [31]. Along the eastern and southern contacts of the massif, gabbroids are intensively tectonized and transformed into amphibolitic blastomylonites [30].

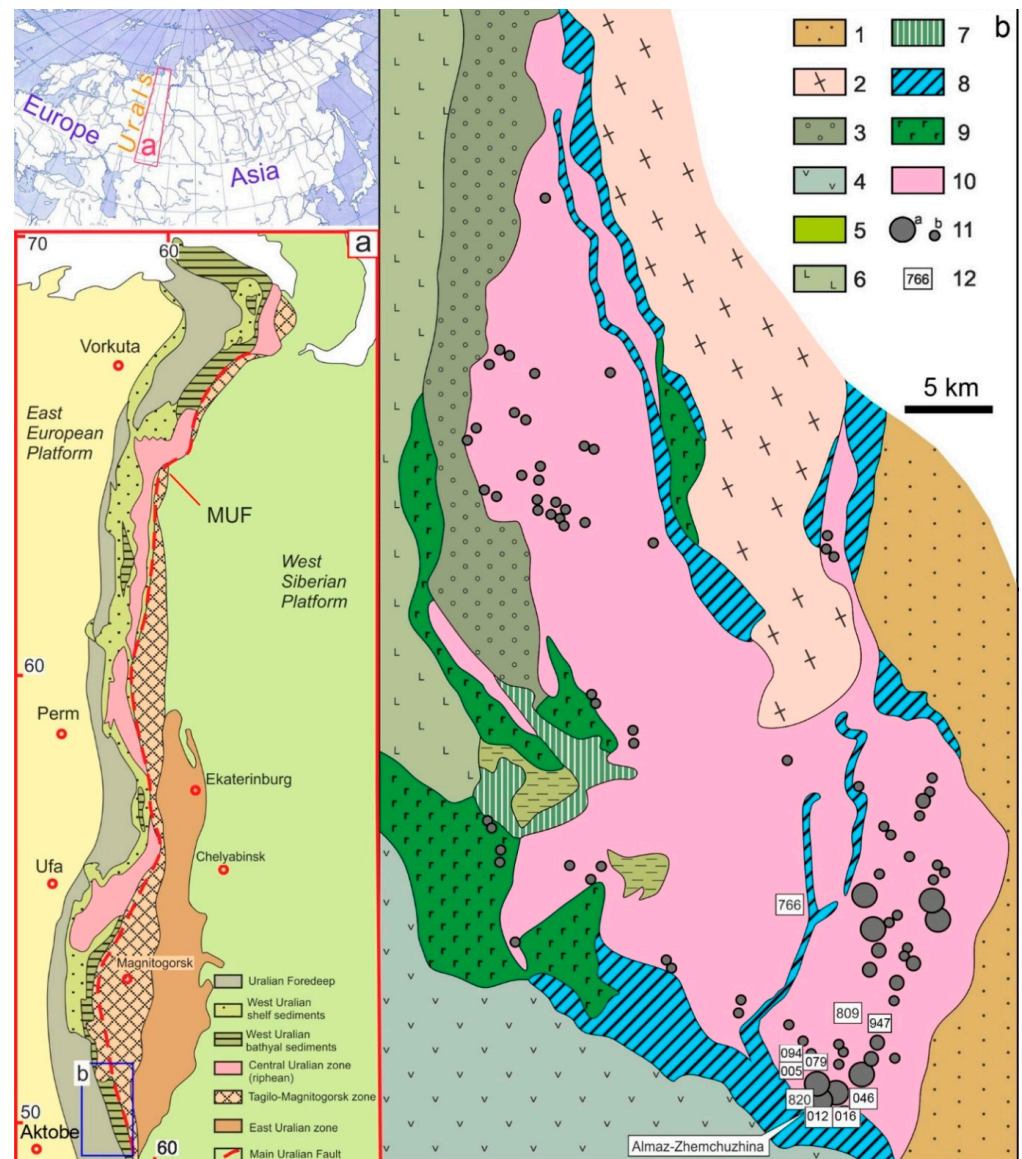


Figure 1. (a) Position of the Kempirsay ophiolite massif within Uralian fold belt (after [32]) and its schematic geological map (after [15,24]) (b): 1–6—Stratified rocks: 1—Yuzhnomugodzhary zone

(basalts (S-D₁, D₂), flyschoids and olistostromes (D₃-C₁); 2—Ebeta zone (basalt-andesite-rhyodacite units, carbonaceous-silicite and greywacke formations (V?PZ₁₋₂); 3–6—Sakmara zone: 3—basalt-andesite-dacite units, greywacke phthanite and carbonate formations (PZ₁₋₂), 4—pillow lavas and pyroclastics of basalt-andesite-rhyodacite units with members of phtanites and clay-siliceous shales (PZ₁₋₂), 5—phtanites and carbonaceous shales (O₂), 6—tholeiite pillow basalts with phtanite lenses (O₂), 7–10—Kempirsay massif: 7—swarms of parallel diabase dykes and isotropic hornblende gabbro, 8—Kyzylkain unit of pyroxenite-gabbro rocks, 9—Kokpekta unit of olivine gabbro and troctolite, 10—upper mantle harzburgite, lherzolite and dunite, 11—chromitites (a—unique and large deposits; b—ordinary deposits and occurrences; icon size correlates with ore reserves), 12—numbers of holes from which samples were studied: 766 (samples 7087, 8156), 820 (sample 820/300), 809 (sample 809/347), 012 (sample 012/300.9), 046 (sample 046/359.5), 016 (samples 016/925 and 016/1108.5), 079 (sample 079/90.7), 005 (sample 005/263.6), 094 (sample 094/238.7), 947 (sample 947/540).

Chromitite deposits within the Kempirsay massif occur extremely irregularly. Although there are four ore fields in total, i.e., the Main, Batamshinsk, Stepninsk, Mamyt, all commercially valued deposits of high-Cr ores are clustered in the Main ore field (MOF). In other ore fields, there are relatively small ore deposits with prevalent aluminous (Batamshinsk) and ferruginous (Stepninsk) Cr-spinels [15].

The MOF is located in the south-eastern part of the massif and spatially coincides with the area of the dunite-harzburgite unit. Chromitite deposits are localized within dunite bodies of varied thicknesses, sometimes occur among harzburgites, but are always separated from the latter by at least a thin dunite envelope. The Dzharlybutak is the largest ore node in the MOF, comprising the world's largest ophiolite-type chromitite deposit called the Almaz-Zhemchuzhina (Figure 1) and several other deposits, i.e., the Pervomayskoye, Millionnoye, Geofizicheskoe-VII and smaller ones.

As shown by previous researchers [33], ore zones are structurally similar to bunches thickening at depth and scattering towards the surface. In particular, within the Dzharlybutak ore node, in the upper parts of the section, the ore bunches are extensive and branched; a larger number of ore bodies are noted here, their morphology is more complex, while the ores are less clustered, poor- and medium-disseminated chromitites prevail. At deeper levels, ore bunches become smaller in volume and less complicated structurally, but at the same time, the ore concentration increases, and densely disseminated and massive chromitite get prevalent.

3. Materials and Methods

Field study and sampling of ultramafic rocks in the south-eastern part of the Kempirsay massif was conducted by intersecting and investigating dumps of the Almaz-Zhemchuzhina and Yuzhnoye deposits. However, due to abundant signatures of secondary changes in rocks, the most important primary material was obtained from the study of the core material from deep boreholes drilled in the area of the Dzharlybutak ore cluster (Almaz-Zhemchuzhina and Geofizicheskoe-VII deposits).

The petrographic study of the samples was carried out by standard methods of optical microscopy in transmitted and reflected light (microscopes Polam R-311, Olympus BX-51). The bulk chemical composition of 23 lherzolite samples was analyzed in Chemical Laboratory of the Institute of Geology, Ufa Federal Research Center, Russian Academy of Sciences (IG UFRS RAS, Ufa, Russia). The SiO₂, Al₂O₃, TiO₂, and P₂O₅ contents were determined by photometry, Na₂O and K₂O contents were measured in flame photometer, the FeO + Fe₂O₃ content was analyzed by volumetric method, CaO and MgO contents were determined by titration and losses on ignition (LOI) were measured by weight method. The compositions of rocks are given in Table 1.

Table 1. Bulk rock composition of Kempirsay peridotites (wt.%).

#	Sample	SiO ₂	TiO ₂	Al ₂ O ₃	Fe ₂ O ₃	FeO	CaO	MgO	Na ₂ O	K ₂ O	P ₂ O ₅	LOI	Total
1	809/347	41.0	0.06	1.33	5.10	2.0	2.0	37.0	0.20	0.1	0.02	11.90	100.71
2	2B/1020	36.6	0.06	0.75	3.89	2.0	0.9	39.2	0.20	0.1	0.01	16.30	100.01
3	947/640	37.0	0.90	1.00	4.00	1.0	1.2	37.0	0.25	0.1	0.01	17.20	99.96
4	820/300	38.5	0.06	1.71	5.90	3.86	3.4	33.6	0.20	0.1	0.01	12.20	99.54
5	005/1159	38.5	0.06	1.70	4.90	3.0	2.0	38.2	0.20	0.1	0.01	11.60	100.27
6	178/370	37.0	0.08	1.20	6.40	1.8	2.0	37.0	0.20	0.1	0.01	14.00	99.79
7	8156	43.0	0.10	1.33	4.00	5.8	2.0	42.0	0.10	0.1	0.14	2.00	100.57
8	016/1108.5	39.0	0.06	1.33	7.00	1.6	1.4	38.0	0.20	0.1	0.01	11.00	99.70
9	016/1108.6	39.0	0.06	2.00	7.00	1.44	1.2	38.0	0.20	0.1	0.01	10.78	99.79
10	046/180.0	35.0	0.22	0.25	12.50	5.0	1.4	35.0	0.20	0.1	0.01	11.00	100.68
11	016/360.2	37.4	0.06	0.95	6.00	3.8	1.4	38.4	0.20	0.1	0.01	11.80	100.12
12	094/300.6	37.0	0.06	0.95	6.40	2.55	0.9	38.0	0.20	0.1	0.01	13.50	99.67
13	012/300.9	36.0	0.06	0.95	6.20	2.0	1.4	38.0	0.20	0.1	0.01	15.40	100.32
14	016/765.1	37.0	0.06	0.95	4.79	2.8	1.4	39.0	0.20	0.1	0.01	13.78	100.09
15	046/359.5	36.0	0.06	0.95	6.70	3.2	1.4	38.0	0.20	0.1	0.01	13.90	100.52
16	Ke-03	37.0	0.01	0.80	6.41	1.83	1.4	38.0	0.20	0.1	0.01	14.50	100.26
17	Ke-04/3	37.0	0.03	0.76	5.80	1.9	1.2	39.0	0.20	0.1	0.01	14.10	100.10
18	Ke-07	37.0	0.10	1.00	6.00	2.5	1.4	37.0	0.20	0.1	0.01	14.20	99.51
19	Ke-08	37.0	0.10	1.01	6.10	0.4	1.0	39.0	0.20	0.1	0.01	14.50	99.42
20	Ke-21	37.0	0.10	1.06	6.80	0.4	1.0	38.0	0.20	0.1	0.01	15.00	99.67
21	Ke-22	37.0	0.10	0.76	4.60	1.6	0.5	39.0	0.20	0.1	0.01	16.00	99.87

The composition of rock-forming silicates and accessory Cr-spinels was determined by X-ray spectral analysis. The studies were carried out on a Tescan Vega 4 Compact scanning electron microscope (SEM) with an Oxford Instruments Energy Dispersive X-Ray (EDX) spectroscope (Xplore 15) at the Institute of Geology UFRS RAS (Ufa, Russia). The spectra were automatically processed using the AzTec software package employing the TrueQ technique. The electron beam accelerating voltage was 20 kV, with a current of 3 nA and a beam size of 3 μ m. X-ray acquisition time was 60 s or 106 impulses in “Point&ID” regime. Quantification of elemental compositions was conducted using standard samples of natural and synthetic compounds. In some lherzolite samples, SEM-EDS analyzes were performed in normalization mode to 100%.

The details of the internal structure of two fresh lherzolite samples (7087, 8156) were revealed by electron backscatter diffraction (EBSD) technique on a Hitachi S-3400N SEM equipped with an Oxford NordlysNano EBSD detector at the GEOMODEL Resource Centre (St. Petersburg State University, St. Petersburg) at a 30-kV accelerating voltage, a 5-nA beam current and a beam focused to a point not exceeding 100 nm. The EBSD patterns were recorded in the form of reflection of an incident electron beam from a 70° pre-tilted sample on a luminescent screen. The fact that a diffraction event is spatially limited by beam size on the surface and several tens of nanometers in depth makes EBSD a highly localized method for microstructure investigations. Acquired patterns were automatically indexed using Oxford AztecHKL software with predefined phases (olivine ICSD 9334; orthopyroxene ICSD 37313) in a Hough space with a resolution of 150. All matching solutions are characterized by an error value of mean angle deviation (MAD) from theoretical diffraction pattern and a number of matching bands. The MAD values rarely exceed 0.6°, which is considered a good match.

4. Results

4.1. Petrographic Features of Ultramafic Rocks and Chromitites

Like in most ultramafic massifs of the ophiolite assemblages in the Southern Urals, completely serpentinized rocks dominate on the surface of the Kempirsay massif. At the same time, a low-temperature type of serpentinization (mesh texture) occurs almost universally, which allowed to preserve relic structures of ultramafic rocks (Figure 2a,b). Primary silicate minerals (olivine, pyroxene) are completely replaced by serpentine, while the composition of accessory Cr-spinel remained mainly unaltered.

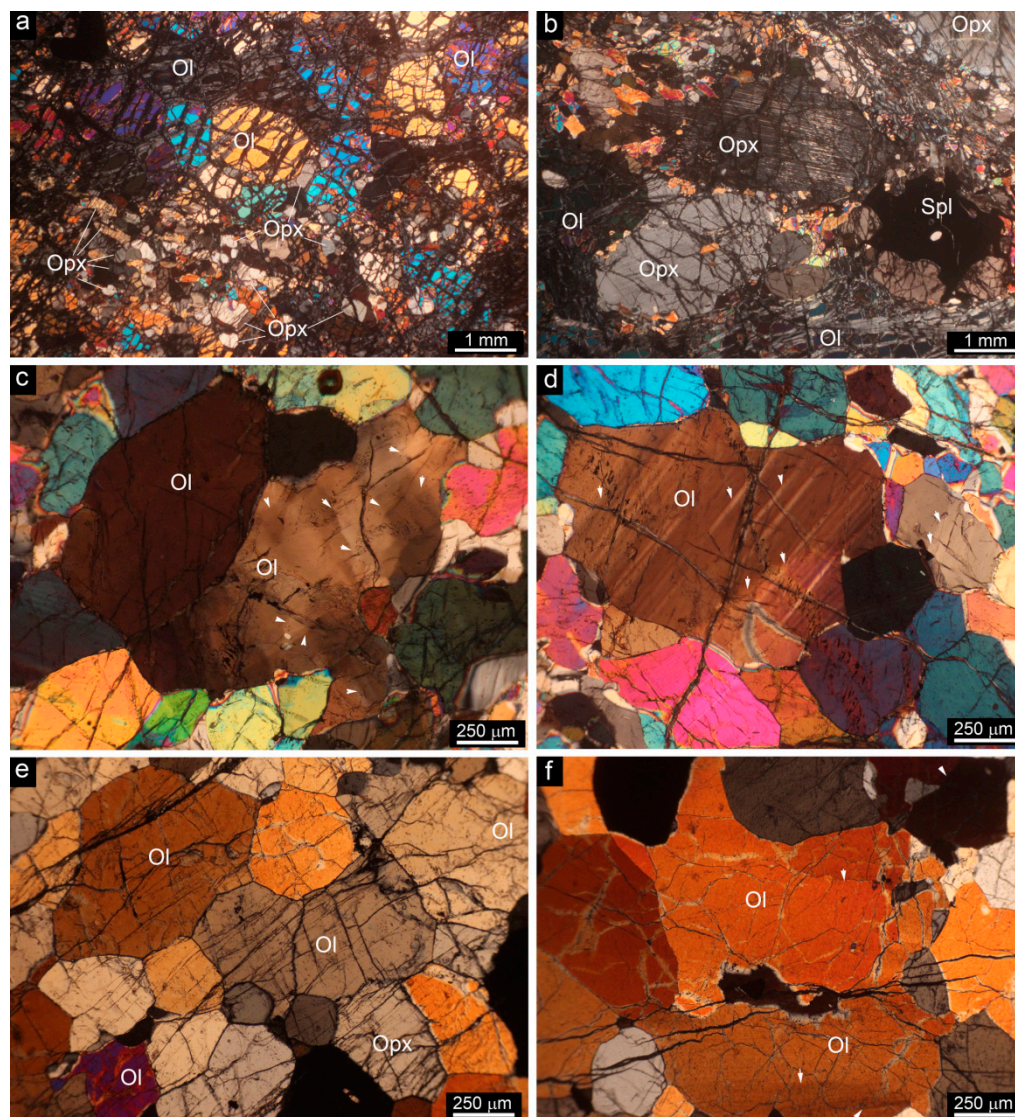


Figure 2. Petrographic features of peridotites from Kempirsay massif: (a)—Protogranular structure in predominantly olivine aggregate of lherzolite with secondary mesh serpentine (sample 820/300); (b)—Porphyroclastic structure on the area with predominant enstatite grains in lherzolite (sample 809/347); (c)—Undulose extinction of olivine grain reflecting a subgrain structure development that induced by plastic deformation (sample 8156); (d)—Parallel-alternating extinction in plastically deformed olivine grains which surrounded by recrystallized neoblasts in fresh lherzolite (sample 8156); (e)—Polygonal-grained olivine aggregates (sample 7087); (f)—Anhedronal olivine grain separated by subgrain boundaries in polygonal-grained aggregate (sample 7087). Arrows note subgrain boundaries. Ol—olivine, Opx—orthopyroxene, Spl—Cr-spinel.

The primary composition of fully serpentinized rocks can be recognized by the presence of bastite pseudomorphs, which mark the presence of orthopyroxene grains in the protolith, as well as by the morphological and chemical features of accessory spinels. These features considered, lherzolititic and harzburgitic serpentinites predominate among the studied ones.

We managed to find the freshest samples of spinel peridotites in the core of boreholes 766, 809, 820, which will be discussed in more detail below. Among the studied samples, two structural types are distinguished: peridotite samples 809/357 and 820/300 are represented by a porphyroclastic structure, while samples 7087 and 8156 from deep borehole 766 show a granoblastic structure.

Peridotites of both types show clear signatures of high-temperature deformation of orthopyroxene and olivine, which are expressed in kink-band structures, undulose extinction, bending of planar structural elements: lamellae, orthopyroxene cleavage (Figure 2c,d). Porphyroclastic peridotites consist of rare, relatively large, deformed enstatite grains surrounded by smaller grains of enstatite, diopside and olivine. Lherzolite samples with granoblastic structure (7087, 8156) contain almost no serpentine; olivine and enstatite grains are mainly equiaxial. Elongated olivine grains separated by deformation bands are rare here. In general, polygonal grains with triple junctions at angles close to 120° (Figure 2e,f) prevail. It is typical of grains subject to secondary recrystallization, once the system tends to minimize grain boundary energy (e.g., [34,35]). A distinctive structural feature of large enstatite porphyroclasts is intensely developed numerous inclusions of other phases, i.e., diopside, pargasite and Cr-spinel (Figure 3a–d). Thus, ultramafic rocks occur in fresh lherzolites from borehole 766 at the depth of more than 1000 m, showing traces of high-temperature deformation, syntectonic recrystallization and annealing recrystallization.

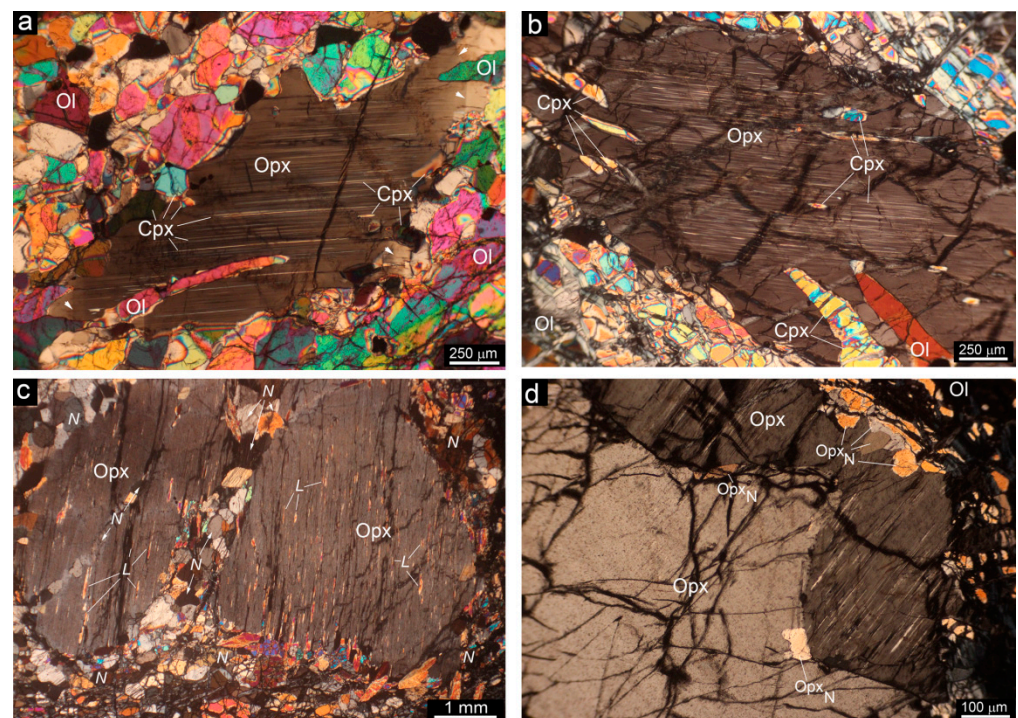


Figure 3. Structural and morphological features of pyroxene grains in lherzolites from Kempirsay massif: (a,b)—Deformation of Opx porphyroclast according with impregnation along shear zones olivine and diopside, and a deformation-induced formation of lamellae and neoblasts of diopside and pargasite (a—sample 7087, b—sample 016/1108.5); (c)—Deformed Opx porphyroclast with abundant lamellae (L) of diopside, pargasite, spinel, and a neoblast cluster (N) along shear zones (arrows) (sample 820/300); (d)—Initial stage of neoblast formation along blocks boundary and close to grain edges in deformed Opx grain (sample 809/347). Cpx—clinopyroxene.

The morphology of Cr-spinel grains varies from amoeboid, vermicular and holly-leaf in lherzolites to subhedral in harzburgites (Figure 4a–d). A similar pattern is observed in many ophiolite massifs and upper mantle xenoliths (e.g., [17,36–38]). Many accessory spinel grains contain inclusions of olivine, orthopyroxene, clinopyroxene, and pargasite. In addition, there are numerous fragments of silicate mineral grains incompletely captured by branches of xenomorphic spinel grains (Figure 4a–d). We had formerly noted similar features in lherzolite massifs of the Southern Urals [11,23]. In dunites and dunitic serpentinites mainly found close to ore deposits, Cr-spinel grains show a nearly euhedral habit (Figure 4g,h). However, their characteristic features are smooth boundaries and the presence of cracks along grains commonly perpendicular to foliation and banding of rocks.

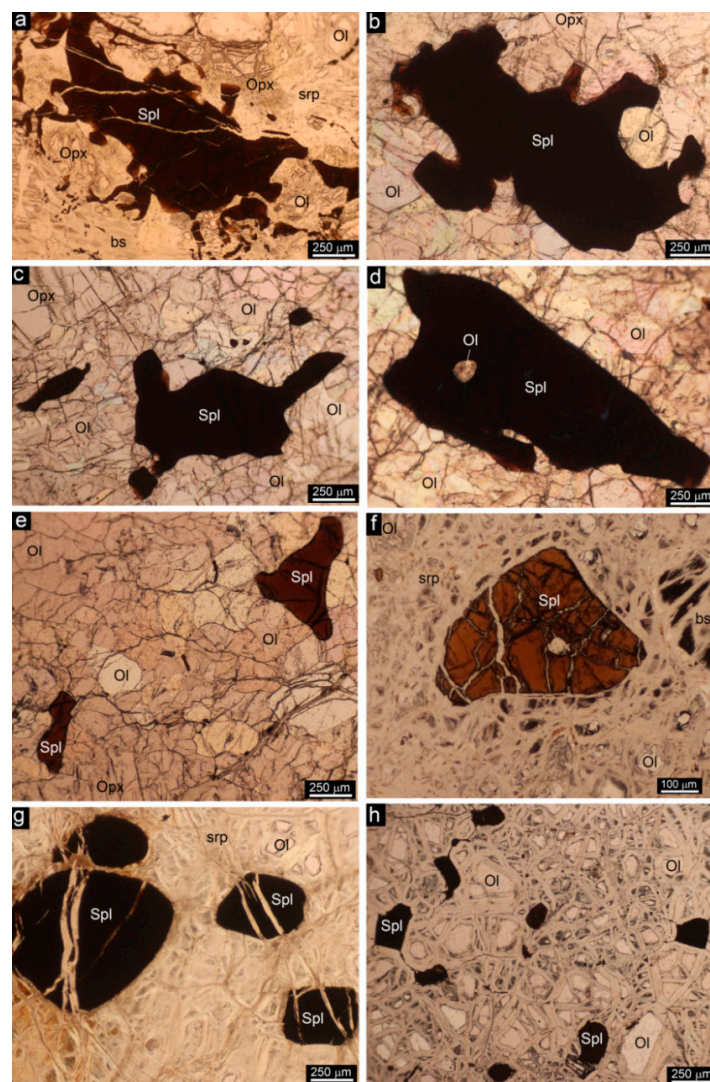


Figure 4. Morphological features of accessory spinel grains from ultramafic rocks of Kempirsay massif: (a,b)—Anhedral Cr-spinel grains (holly leaf) with silicate inclusions, as well as units of ol-spl and opx-spl “symplectites” close to them (a—sample 809/347, b—sample 8156); (c)—Unequally-grained Cr-spinels in lherzolite: fine-grained euhedral and subhedral grains, and large anhedral grain with branches (sample 7087); (d)—Large anhedral Cr-spinel grain containing inclusions and occupying silicate fragments in lherzolite (sample 7087); (e)—Subhedral and elongated Cr-spinel grains in fresh spinel peridotite (sample 7087); (f)—Subhedral Cr-spinel grain in serpentinitized harzburgite (sample 012/300.9); (g)—Isometric smooth Cr-spinel grains in dunitic serpentinite (sample 947/540); (h)—Subhedral and euhedral Cr-spinel grains in serpentinitized dunite (sample 046/359.5). bs—bastite, srp—serpentine.

Chromitites show a further change in the morphology of Cr-spinel grains. Poorly disseminated chromitites are composed of small grains of chromite (0.1–0.5 mm) with smooth contours (Figure 5a). Many grains are broken by cracks that are usually perpendicular to the banding of ore bodies. Most chromite grains (80%–85%) have no inclusions; other grains (10%–15%) contain rare round or oval inclusions of olivine, which is in most cases replaced by serpentine, as well as tabular, prismatic or negative crystal inclusions represented by pargasite and rare phlogopite (Figure 5b). Only few Cr-spinel grains (about 1%) contain numerous inclusions, which are mainly represented by pargasite (Figure 5c,d), less often by diopside, enstatite and phlogopite.

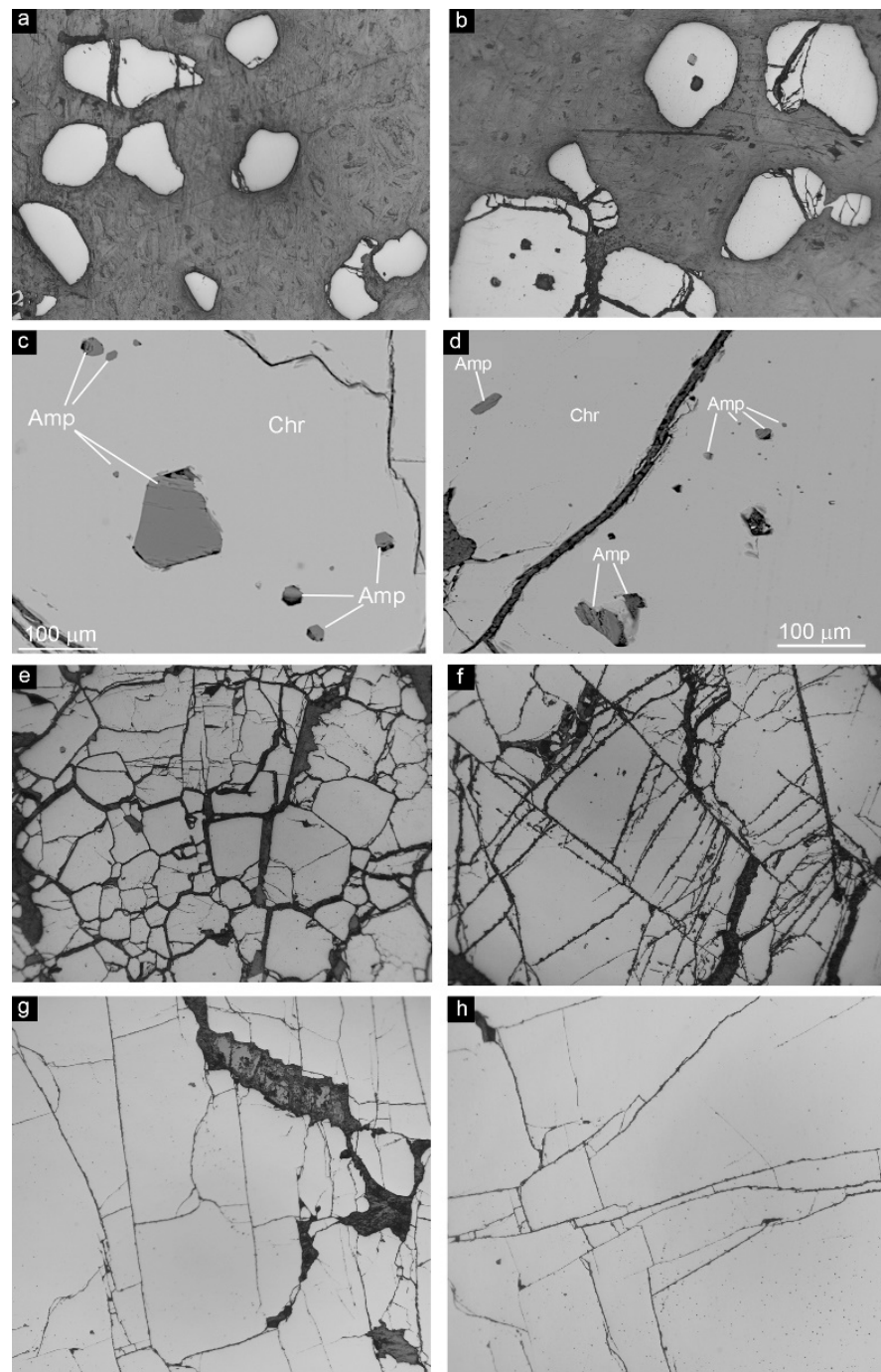


Figure 5. Evolution of chromitite structure in deposits of Kempirsay ophiolite massif: (a)—Sparsely disseminated fine-grained chromitite consisting of small smooth chromite grains (sample 079/90.7);

(b)—Moderately disseminated chromitite: grains containing pargasite and olivine inclusions (sample 079/90.7); (c,d)—Amphibole inclusions in chromite grains (sample 005/263.6); (e)—Densely disseminated chromitite formed by impingement, compaction and coarsening of grains (sample 005/263.6); (f)—Massive coarse-grained chromitite with joints formed by compaction (sample 094/238.7); (g)—Squeezing of weak silicate matrix from between the chromite grains in massive ore and compaction by “pressure sintering” leading to disappearance of boundaries (sample 016/925); (h)—Already homogeneous massive chromitite with rare thin and straight joints as result of “pressure sintering” (sample 016/925). Width of images a,b,e-h is 2 mm. Amp—amphibole, Chr—chromite.

In densely disseminated chromitites, an average grain size increases (0.5–3 mm), the grain shape becomes angular, which indicates adjustment of individuals’ boundaries in consolidation settings (Figure 5e). Transverse and radial cracks become more widespread (Figure 5f), passing through inner parts of grains mainly. Such structural features in chromitites are known as “pull-apart” texture and attributed to the ore formation under tectonic stress conditions [39].

An even greater consolidation is recorded in massive chromitites. It is expressed in the presence of anhedral segregations of vein minerals formed by “squeezing out” of weaker silicate minerals from gaps between rigid chromite grains (Figure 5g). The consolidation is also reflected in sharp thinning and gradual vanishing of boundaries between Cr-spinel grains that become angular-shaped (Figure 5g,h).

Main types of ores: massive and disseminated. Chromitites vary from fine-grained (<1 mm) to coarse-grained (>3 mm), the most typical are densely disseminated ores with 70%–90% chromite grains. Ore styles are banded, schlieren-banded, uniformly disseminated and spotty varieties. Massive chromitites (>90% chromite) are mainly composed of medium- and coarse-grained types (grain size more than 2 mm). Nodular ores are of subordinate importance and are usually found near massive ores, more often along the periphery of ore bodies. Nodules are usually composed of an aggregate of sub- and anhedral grains larger than 2 mm; the cement is completely serpentinized dunite.

4.2. Bulk Rock Composition

Most ultramafic rock samples are largely subject to serpentinization (70%–100%), as evidenced by high levels of loss on ignition (LOI = 10–17 wt.%). Only two of the studied samples demonstrate exceptional freshness, both of them being taken from the core of deep borehole 766 at the depth of more than 1000 m (Table 1). All samples show a composition typical of ophiolite ultramafic rocks, i.e., high contents of MgO (33.6–41.8 wt.%), SiO₂ (36.3–43.08 wt.%) and ΣFeO (6.2–17.5 wt.%) and low concentrations of oxides of other major elements (wt.%): Al₂O₃ (<2), CaO (<3.4), TiO₂ (<1), MnO (<0.1), Na₂O (<0.25), K₂O (<0.1), P₂O₅ (<0.14).

The modal mineral composition in fresh samples of ultramafic rocks (7087 and 8156) corresponds to lherzolite, which is also comparable with the estimate of the normative mineral composition according to chemical analysis data for 8156: Ol–81.5, En–12.5, Di–6%. Due to the intense serpentinization, the rock variety in all of the remaining studied samples was determined based on the chemical composition (Figure 6a). Most of the 20 studied samples were attributed to lherzolites (Lz) and a transitional variety between lherzolite and harzburgite, which we called lherzolite-harzburgite (Lz-Hb). According to the chemical composition, only 3 samples can be referred to as dunites.

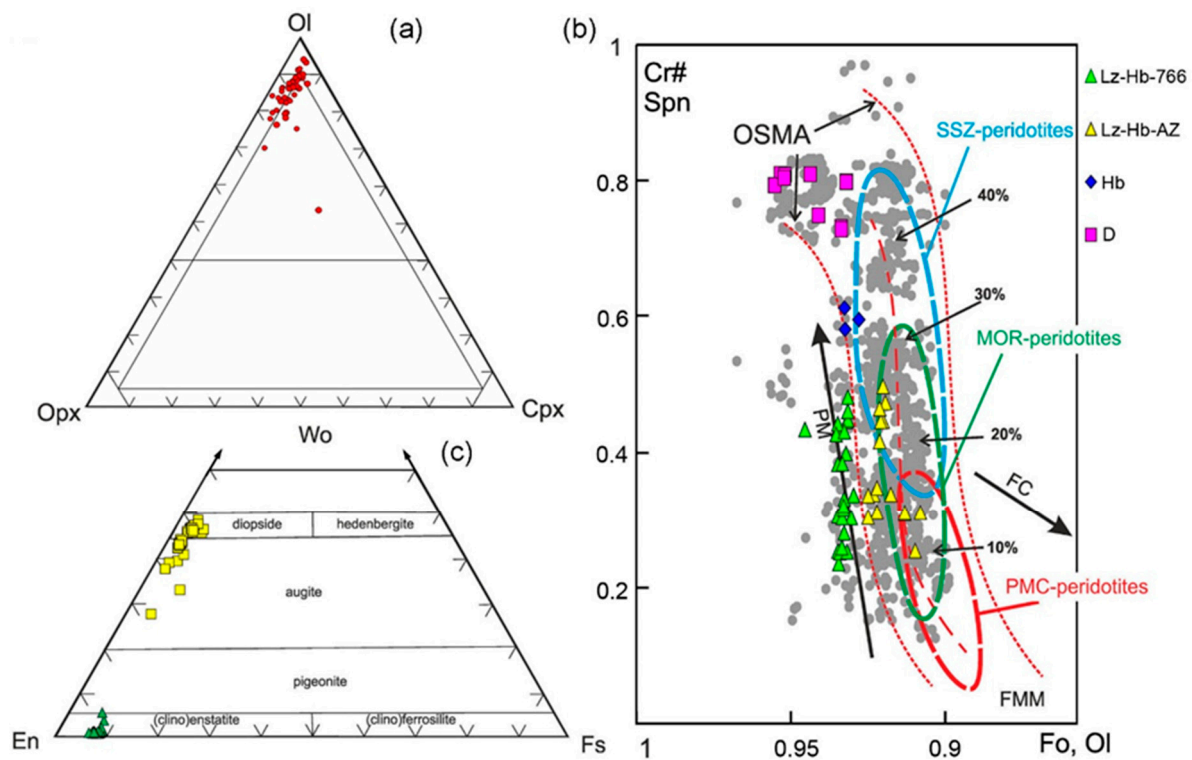


Figure 6. (a)—Normative mineral compositions of peridotites inferred from chemical composition; (b)—OSMA diagram for coexisting Ol and Cr-spl grains; here, percent notes partial melting degree in experiment after [40], that corresponds to Ol-Spl compositions in restite; gray points are Ol-Spl compositions in lherzolite-type massifs of South Urals after [41]; Lz-Hb-766—peridotite of well 766; Lz-Hb-AZ—peridotite from Almaz-Zhemchuzhina deposit area; Hb—harzburgite, D—dunite; (c)—Compositions of Opx and Cpx on the triangular diagram En–Wo–Fs.

4.3. Composition of Minerals

The main primary minerals of the studied ultramafic rocks are high-Mg olivine, orthopyroxene, and Ca-Mg clinopyroxene; Cr-spinel and amphibole are accessory phases. The main secondary mineral is serpentine; chlorite and carbonates are rare. Fe, Ni, Co, Cu, PGE sulfides, native minerals Ni-Fe, Cu and PGE also occur in small amounts as minor segregations in ultramafic rocks and chromitites. In this work, we will focus on description of the main minerals of the primary (upper mantle) assemblages only.

Olivine composes 75% to 100% of the rock volume in lherzolites and dunites, respectively. However, it is most susceptible to serpentinization and, therefore, is almost not preserved in the upper parts of the massif, giving way to mesh serpentine. In the studied samples, its content varies from complete absence to 10%–50%, and only in samples from borehole 766 is it almost completely preserved and makes up 75%–80% of the rock.

The olivine is exclusively magnesian and varies from 91 at.% to 95 at.% of the forsterite (Fo) end-member (Table 2). Notably, grains included in ore chromite are highest in Mg, while some lherzolite samples are lowest in Mg. However, it should be noted that there is no clear relationship between the Mg content of olivine and the Cr-number (#Cr) of accessory spinel, as implied by fields in the OSMA diagram (Figure 6b). Among the studied samples, the least magnesian olivines were found in peridotites of the MOF (Fo_{91–92}), while rather high-Mg olivines coexist with high-Al spinels (Fo_{93–94}) in fresh lherzolites of borehole 766.

Orthopyroxene is the second major mineral in lherzolites and harzburgites. In dunites it often occurs as a minor phase (less than 5%), such rocks are often called pyroxene- (or enstatite-) dunites [14]. It is also subject to serpentinization with bastite pseudomorphs produced, but sometimes it is replaced by amphibole. Orthopyroxene is high-Mg with an enstatite end-member content of 91–93 at.% (Table 3, Figure 6c). The usual minor elements

of Opx are Ca, Al and Cr. In fact, the following regularity is established: large enstatite porphyroclasts are higher in Al, Cr and Ca (2.5–3/0.6–0.8/0.5–0.8 wt.%, respectively) compared to their concentrations in neoblasts (0.9–1.5/0.2–0.5/0.3–0.6 wt.%, respectively) formed during syntectonic recrystallization of deformed grains.

Table 2. Composition of olivine grains in peridotite of Kempirsay massif (wt.%).

#	1	2	3	4	5	6	7	8	9	10	11	12	13	14	15	16	17
Rock	Lz	Lz	Lz	Lz	Lz	Lz	Lz-Hb	Lz-Hb	Lz-Hb	Lz-Hb	Hb	Hb	D	D	D	D	D
SiO ₂	40.38	40.26	40.55	40.65	40.46	40.66	40.33	40.67	40.18	40.95	39.96	40.46	40.95	41.76	41.10	40.69	40.56
FeO	7.09	7.15	6.95	7.10	6.76	5.65	8.24	8.19	8.10	8.59	7.39	6.96	4.85	5.05	5.03	6.12	6.88
MnO	0.19	bdl	bdl	bdl	bdl	bdl	bdl	bdl	bdl	bdl	0.19	bdl	bdl	bdl	bdl	bdl	bdl
MgO	51.97	52.34	52.19	51.93	52.46	52.64	50.78	50.97	50.68	51.15	51.03	51.60	53.45	53.97	53.95	52.53	51.95
NiO	0.37	0.25	0.32	0.33	0.32	0.35	0.29	0.41	0.28	0.41	0.29	0.42	0.48	0.36	0.52	0.36	0.28
Total	100.0	100.0	100.0	100.0	100.0	100.0	99.65	100.24	99.24	101.10	98.88	99.43	99.73	101.14	100.60	99.70	99.67
Si	0.975	0.970	0.978	0.981	0.974	0.982	0.982	0.985	0.982	0.985	0.978	0.982	0.982	0.989	0.977	0.981	0.981
Fe	0.143	0.144	0.140	0.143	0.136	0.114	0.168	0.166	0.165	0.172	0.151	0.141	0.097	0.100	0.100	0.123	0.139
Mn	0.004	0	0	0	0	0	0	0	0	0	0.005	0	0	0	0	0	0
Mg	1.871	1.881	1.876	1.869	1.884	1.897	1.844	1.841	1.847	1.835	1.861	1.868	1.911	1.905	1.913	1.889	1.874
Ni	0.007	0.005	0.006	0.006	0.006	0.007	0.006	0.008	0.006	0.008	0.006	0.008	0.009	0.007	0.010	0.007	0.005
Fo	0.93	0.93	0.93	0.93	0.93	0.94	0.92	0.92	0.92	0.91	0.92	0.93	0.95	0.95	0.95	0.94	0.93
Fa	0.07	0.07	0.07	0.07	0.07	0.06	0.08	0.08	0.08	0.09	0.08	0.07	0.05	0.05	0.05	0.06	0.07

bdl = below detection limit.

Clinopyroxene occurs as an accessory mineral in some samples of dunites and harzburgites (up to 5%), while in lherzolites it is present mainly as small grains (10–100 µm) in the amount of 5%–8%. Large grains of clinopyroxene are very rare. It is often found in association with Cr-spinel grains or close to large orthopyroxene porphyroclasts. The studied clinopyroxene grains are represented by the Ca-Mg variety (Table 4). On the triangular diagram their compositions fall into the field of diopside mainly and only a small part of the analyses is interpreted as augite (Figure 6c). The main impurities are aluminum (0.74–3.26 wt.% Al₂O₃) and chromium (0.25–1.29 wt.% Cr₂O₃), single analyses show the presence of sodium (up to 0.2 wt.% Na₂O) and titanium (up to 0.3 wt.% TiO₂).

Amphibole is found in minor amounts (0.1–2%) in lherzolites, usually occurring inside deformed enstatite grains as lamellae or as small prismatic grains along their periphery in association with small grains of olivine, ortho- and clinopyroxene. Amphibole typically shows a very consistent composition and corresponds to the Mg-Ca variety—Pargasite (Table 5), which constant minor elements are sodium and chromium. Their amount ranges from 0.8 to 3 wt.% of the corresponding oxide.

Cr-spinel is a constant accessory mineral in all varieties of ultramafic rocks and the major mineral of chromitites. Its content in lherzolites and harzburgites varies from tenths of a percent to 3%–5%, while in dunites there are wider variations up to the formation of ore concentrations (disseminated chromitites contain > 20% chromite).

Cr-spinel grains are characterized by widely varied compositions (Table 6; Figure 7a,b) expressed both in the change of ratios between trivalent cations (mainly Cr/Al) and divalent cations (Mg/Fe). The content of trivalent iron in accessory spinel grains is insignificant and slightly increases in host dunites and chromitites. The further growth of Fe³⁺ is associated with the metamorphism of ultramafic rocks and chromitite, which is no typical phenomenon for the Kempirsay massif.

Table 4. Composition of clinopyroxene grains in peridotite of Kempirsay massif (wt.%).

#	1	2	3	4	5	6	7	8	9	10	11	12	13	14	15	16	17	18	19
Rock	Lz	Lz	Lz	Lz	Lz-Hb	Lz-Hb	Lz-Hb	Lz-Hb	Lz-Hb	Lz-Hb	Lz-Hb	Lz-Hb	Lz-Hb	Lz-Hb	Lz-Hb	Lz-Hb	Lz-Hb	Hb	Hb
SiO ₂	55.22	55.13	55.25	54.47	53.96	53.53	53.29	53.66	53.72	54.00	52.26	53.85	53.16	52.69	52.31	53.36	52.97	52.91	53.10
Al ₂ O ₃	1.10	1.09	1.17	2.14	0.74	1.03	1.51	1.58	1.60	0.99	2.93	3.26	1.09	1.62	2.84	1.87	2.15	1.09	0.80
FeO	1.57	1.57	1.48	1.53	1.67	1.80	2.03	1.85	2.04	1.94	1.72	2.02	1.68	2.35	1.85	1.88	2.16	1.59	1.49
MgO	19.79	20.01	19.67	19.17	18.40	18.23	18.10	18.02	18.18	18.45	17.52	17.30	18.62	17.58	17.55	17.93	17.90	18.30	18.30
CaO	22.05	21.95	22.14	21.96	23.83	23.74	23.35	23.35	23.25	23.67	23.03	24.58	23.14	24.29	22.78	23.16	23.17	23.0	23.0
Cr ₂ O ₃	0.27	0.25	0.29	0.72	0.32	0.32	0.41	0.50	0.44	0.28	0.85	1.29	0.39	0.31	0.89	1.01	0.95	0.54	0.53
Total	100	100	100	100	98.92	98.66	98.69	98.96	99.24	99.33	98.32	102.30	98.09	98.85	98.22	99.20	99.30	97.43	97.22
Si	1.982	1.979	1.982	1.957	1.974	1.965	1.956	1.961	1.959	1.968	1.924	1.914	1.960	1.941	1.927	1.948	1.935	1.963	1.973
Al	0.047	0.046	0.049	0.091	0.032	0.045	0.065	0.068	0.069	0.043	0.127	0.136	0.047	0.070	0.123	0.080	0.093	0.047	0.035
Fe	0.047	0.047	0.044	0.046	0.051	0.055	0.062	0.056	0.062	0.059	0.053	0.060	0.052	0.072	0.057	0.057	0.066	0.049	0.046
Mg	1.059	1.071	1.052	1.027	1.004	0.998	0.991	0.982	0.989	1.003	0.961	0.917	1.024	0.966	0.964	0.976	0.975	1.013	1.014
Ca	0.849	0.845	0.853	0.847	0.935	0.935	0.920	0.916	0.910	0.926	0.910	0.937	0.916	0.960	0.901	0.907	0.908	0.916	0.917
Cr	0.008	0.007	0.008	0.021	0.009	0.009	0.012	0.014	0.013	0.008	0.025	0.036	0.012	0.009	0.026	0.029	0.027	0.016	0.015
En	0.54	0.55	0.54	0.54	0.50	0.50	0.50	0.50	0.50	0.50	0.50	0.48	0.51	0.48	0.50	0.50	0.50	0.51	0.51
Fs	0.02	0.02	0.02	0.02	0.03	0.03	0.03	0.03	0.03	0.03	0.03	0.03	0.03	0.04	0.03	0.03	0.03	0.02	0.02
Wo	0.43	0.43	0.44	0.44	0.47	0.47	0.47	0.47	0.47	0.46	0.47	0.47	0.49	0.46	0.48	0.47	0.47	0.46	0.46

Table 5. Composition of amphibole grains in peridotite of Kempirsay massif (wt.%).

#	1	2	3	4	5	6	7	8	9	10	11	12	13	14	15
Rock	Lz	Lz	Lz-Hb	Lz-Hb	Lz-Hb	Lz-Hb	Lz-Hb	Lz-Hb	Hb	Hb	D	D	D	D	Chr
SiO ₂	55.47	55.09	54.54	53.60	54.94	54.81	52.93	45.96	56.72	54.62	49.33	52.71	47.46	49.07	50.60
TiO ₂	bdl	bdl	bdl	bdl	bdl	bdl	bdl	0.48	bdl	bdl	0.37	0.39	0.42	0.41	0.45
Al ₂ O ₃	2.49	4.56	4.73	5.67	4.00	4.38	6.24	12.95	2.27	3.81	7.54	4.58	8.86	7.23	6.65
FeO	1.48	1.88	2.36	2.72	2.42	2.45	2.60	2.82	1.78	1.98	1.11	0.73	1.45	1.15	1.29
MgO	21.93	23.88	22.54	22.22	23.19	22.66	21.82	19.25	23.78	23.46	21.65	23.92	20.75	23.20	22.45
CaO	15.23	11.71	12.64	12.60	12.75	12.50	12.69	12.44	12.58	12.45	12.18	10.91	12.89	11.10	11.86
Na ₂ O	bdl	bdl	bdl	bdl	bdl	0.39	0.56	2.09	0.00	0.68	2.76	2.64	2.44	2.80	2.06
K ₂ O	0.17	bdl	bdl	bdl	bdl	bdl	bdl	bdl	bdl	bdl	bdl	bdl	bdl	bdl	bdl
Cr ₂ O ₃	1.04	0.68	1.01	1.01	0.51	0.62	0.99	1.87	0.65	0.81	2.91	1.94	3.59	2.89	2.48
H ₂ O *	2.18	2.20	2.19	2.18	2.19	2.19	2.18	2.14	2.20	2.19	2.15	2.18	2.14	2.16	2.17
Total	100.00	100.00	100.00	100.00	100.00	100.00	100.00	100.00	100.00	100.00	100.00	100.00	100.00	100.00	100.00
K	0.030	0	0	0	0	0	0	0	0	0	0	0	0	0	0
Na ¹	0	0	0	0	0	0	0.020	0.431	0	0.009	0.561	0.313	0.599	0.409	0.312
Na ²	0	0	0	0	0	0.165	0.129	0.135	0	0.171	0.182	0.391	0.063	0.346	0.239
Ca	2.246	1.709	1.854	1.853	1.870	1.835	1.871	1.865	1.836	1.829	1.818	1.609	1.937	1.654	1.761
Mg	4.527	4.876	4.631	4.577	4.762	4.656	4.505	4.042	4.859	4.825	4.525	4.938	4.367	4.842	4.667
Fe	0.170	0.213	0.269	0.311	0.276	0.280	0.298	0.329	0.202	0.226	0.129	0.083	0.170	0.133	0.149
Ti	0	0	0	0	0	0	0	0.050	0	0	0.039	0.041	0.044	0.042	0.047
Cr	0.113	0.073	0.109	0.109	0.056	0.067	0.108	0.207	0.070	0.088	0.320	0.210	0.398	0.318	0.271
Al ^{VI}	0.037	0.229	0.232	0.277	0.166	0.215	0.298	0.568	0.090	0.103	0.109	0.000	0.121	0.012	0.095
Si	7.634	7.499	7.470	7.360	7.521	7.509	7.286	6.435	7.726	7.489	6.873	7.254	6.658	6.828	7.011
Al ^{IV}	0.366	0.501	0.530	0.640	0.479	0.491	0.714	1.565	0.274	0.511	1.127	0.746	1.342	1.172	0.989

Table 6. Composition of Cr-spinel grains in peridotite of Kempirsay massif (wt.%).

#	1	2	3	4	5	6	7	8	9	10	11	12	13	14	15	16	17	18	19
Rock	Lz	Lz	Lz	Lz	Lz	Lz	Lz	Lz	Lz	Lz-Hb	Lz-Hb	Lz-Hb	Lz-Hb	Lz-Hb	Lz-Hb	Lz-Hb	Lz-Hb	Lz-Hb	Lz-Hb
TiO ₂	bdl	bdl	bdl	bdl	bdl	bdl	bdl	bdl	bdl	bdl	bdl	bdl	bdl	0.25	bdl	bdl	bdl	bdl	bdl
Al ₂ O ₃	47.03	46.06	41.90	38.56	36.65	34.66	31.85	30.05	29.77	49.07	46.08	43.66	41.77	34.15	37.69	36.55	31.56	33.50	31.16
FeO	13.72	12.98	14.54	15.82	19.42	16.70	16.29	18.22	18.77	11.08	15.34	16.14	13.23	23.61	13.91	16.21	24.62	17.23	20.38
MnO	bdl	bdl	bdl	bdl	0.41	bdl	bdl	bdl	0.41	bdl	bdl	bdl	bdl	bdl	0.35	bdl	bdl	bdl	bdl
MgO	17.62	17.52	16.24	15.59	13.78	15.08	15.32	13.95	13.32	19.12	16.88	16.22	17.48	13.40	16.42	15.70	11.72	14.37	13.37
Cr ₂ O ₃	21.62	23.21	26.91	28.84	28.91	33.28	36.53	37.53	37.43	19.50	21.85	24.31	27.24	25.90	30.37	30.31	29.64	33.86	32.86
V ₂ O ₃	bdl	0.22	bdl	bdl	0.33	0.28	bdl	0.25	0.30	0.00	0.25	0.21	0.19	0.00	bdl	bdl	0.28	bdl	bdl
NiO	bdl	bdl	bdl	bdl	bdl	bdl	bdl	bdl	bdl	bdl	bdl	bdl	bdl	0.36	bdl	bdl	bdl	bdl	bdl
ZnO	bdl	bdl	0.39	bdl	0.49	bdl	bdl	bdl	bdl	bdl	bdl	bdl	bdl	0.45	bdl	bdl	0.72	bdl	0.44
Total	100.0	100.0	100.0	98.81	100.0	100.0	100.0	100.0	100.0	98.77	100.40	100.52	99.92	98.11	98.74	98.78	98.54	98.96	98.19
Al	1.510	1.485	1.381	1.304	1.252	1.183	1.097	1.052	1.047	1.565	1.487	1.425	1.368	1.200	1.274	1.246	1.127	1.163	1.106
Cr	0.466	0.502	0.595	0.654	0.662	0.762	0.844	0.881	0.882	0.417	0.473	0.532	0.599	0.611	0.688	0.693	0.710	0.788	0.782
Mg	0.715	0.714	0.677	0.666	0.595	0.651	0.667	0.617	0.592	0.771	0.689	0.669	0.724	0.595	0.701	0.677	0.529	0.630	0.600
Fe ³⁺	0.035	0.020	0.011	0.039	0.075	0.059	0.050	0.072	0.062	0.025	0.047	0.043	0.026	0.177	0.045	0.073	0.135	0.053	0.106
Fe ²⁺	0.273	0.274	0.327	0.336	0.388	0.339	0.342	0.372	0.399	0.223	0.299	0.326	0.279	0.391	0.284	0.311	0.474	0.366	0.396
Ti	0	0	0	0	0	0	0	0	0	0	0	0	0	0.006	0	0	0	0	0
Mn	0	0	0	0	0.010	0	0	0	0	0	0	0	0	0	0	0	0	0	0
Ni	0	0	0	0	0	0	0	0	0	0	0	0	0	0.009	0	0	0	0	0
V	0	0.005	0	0	0.008	0.007	0	0.006	0.007	0	0.005	0.005	0.004	0	0	0	0.007	0	0
Zn	0	0	0.009	0	0.011	0	0	0	0	0	0	0	0	0.011	0	0	0.018	0	0.011
#Cr	0.24	0.25	0.30	0.33	0.35	0.39	0.43	0.46	0.46	0.21	0.24	0.27	0.30	0.34	0.35	0.36	0.39	0.40	0.41
#Mg	0.72	0.72	0.67	0.66	0.61	0.66	0.66	0.62	0.60	0.78	0.70	0.67	0.72	0.60	0.71	0.69	0.53	0.63	0.60
#	20		21	22	23	24	25		26	27	28	29	30	31	32	33	34	35	36

Table 6. Cont.

#	1	2	3	4	5	6	7	8	9	10	11	12	13	14	15	16	17	18	19
Rock	Lz-Hb	Lz-Hb	Lz-Hb	Lz-Hb	Lz-Hb	Hb	Hb	Hb	D-Hb	D	D	D	D	D	D	D	D	Chr	Chr
TiO ₂	bdl	bdl	bdl	bdl	bdl	bdl	bdl	bdl	0.25	0.28	bdl	bdl	bdl	bdl	bdl	bdl	bdl	bdl	bdl
Al ₂ O ₃	30.03	22.68	26.11	22.81	18.35	17.42	16.46	9.74	9.43	8.73	8.59	8.16	7.41	7.13	6.75	9.34	8.96		
FeO	17.81	30.74	20.55	24.26	24.13	24.18	23.44	18.22	22.06	17.34	18.41	15.21	18.91	19.72	22.98	13.73	12.54		
MgO	13.85	9.17	11.83	11.48	10.12	10.17	10.42	11.67	10.05	12.37	11.40	13.50	11.32	11.27	9.28	14.87	15.35		
Cr ₂ O ₃	37.34	34.61	41.20	39.43	44.94	45.82	47.30	57.47	55.03	58.97	58.86	60.99	60.33	60.76	59.70	60.03	61.02		
V ₂ O ₃	0.25	0.25	0.28	0.26	0.31	bdl	0.31	bdl	bdl	bdl	bdl	bdl	bdl	bdl	bdl	0.24	bdl	bdl	
Total	99.28	97.89	99.97	98.25	97.85	97.59	97.92	97.34	96.86	97.41	97.26	97.86	97.97	98.87	98.94	97.96	97.86		
Al	1.058	0.864	0.940	0.848	0.704	0.672	0.635	0.385	0.380	0.345	0.343	0.319	0.295	0.282	0.271	0.360	0.345		
Cr	0.882	0.885	0.995	0.983	1.156	1.186	1.223	1.524	1.485	1.562	1.573	1.601	1.611	1.612	1.608	1.551	1.576		
Mg	0.617	0.442	0.539	0.540	0.491	0.496	0.508	0.583	0.511	0.617	0.574	0.668	0.569	0.563	0.471	0.724	0.747		
Fe ³⁺	0.066	0.248	0.059	0.156	0.136	0.139	0.143	0.091	0.119	0.094	0.097	0.087	0.082	0.099	0.107	0.097	0.092		
Fe ²⁺	0.372	0.556	0.460	0.466	0.506	0.507	0.482	0.410	0.498	0.382	0.412	0.326	0.443	0.444	0.536	0.268	0.241		
Ti	0	0	0	0	0	0	0	0.006	0.007	0	0	0	0	0	0	0	0	0	0
V	0.006	0.006	0.007	0.007	0.008	0	0.008	0	0	0	0	0	0	0	0	0	0	0	0
#Cr	0.45	0.51	0.51	0.54	0.62	0.64	0.66	0.80	0.80	0.82	0.82	0.83	0.85	0.85	0.86	0.81	0.82		
#Mg	0.62	0.44	0.54	0.54	0.49	0.49	0.51	0.59	0.51	0.62	0.58	0.67	0.56	0.56	0.47	0.73	0.76		

#Cr = Cr/(Cr + Al), at.%; #Mg = Mg/(Mg + Fe²⁺), at.%.

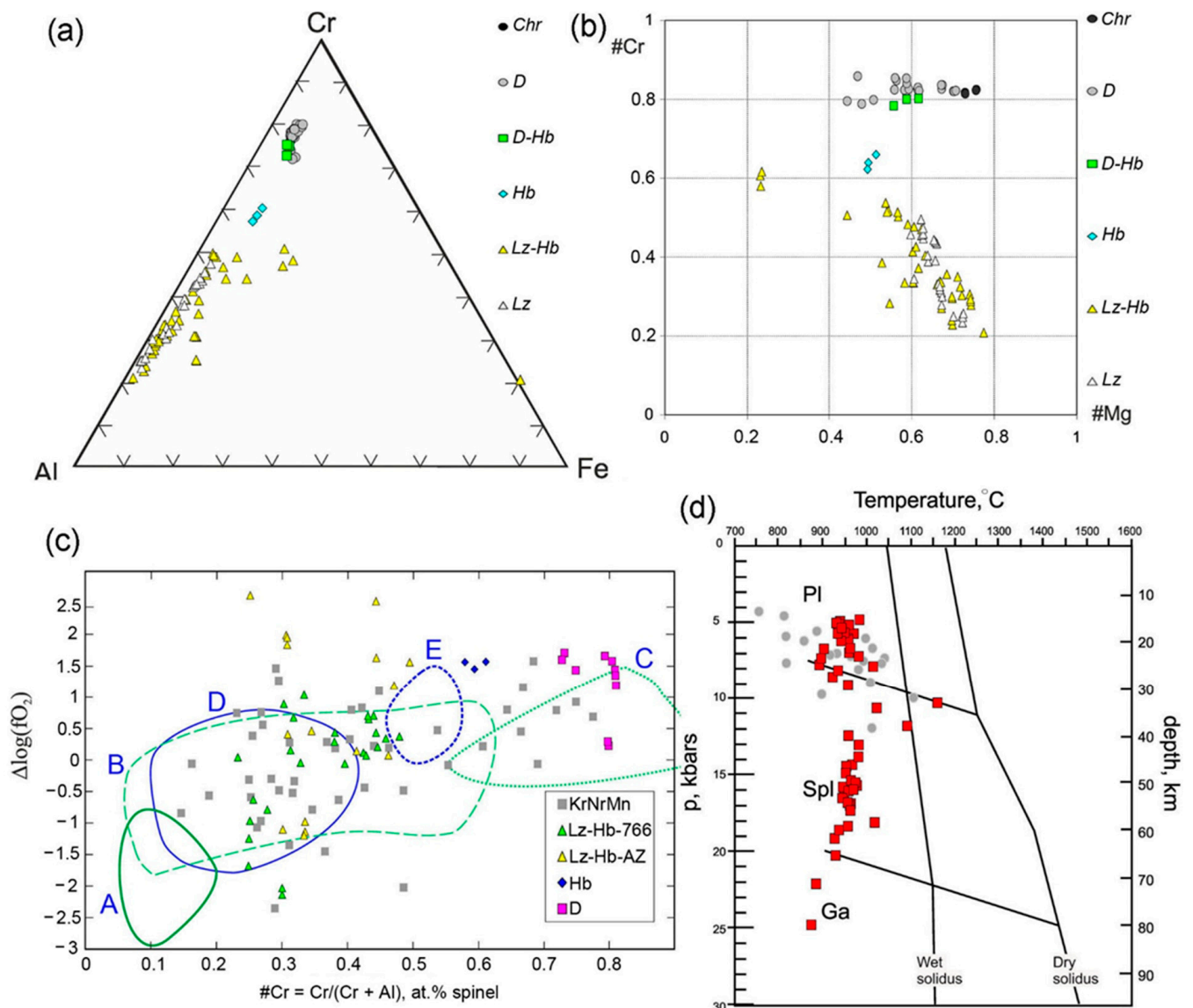


Figure 7. (a)—Al–Cr–Fe diagram for three-valent cations of Cr-spinel; (b)— $\#Cr = Cr/(Cr + Al)$ vs. $\#Mg = Mg/(Mg + Fe)$ diagram for Cr-spinel grains; (c)— $\#Cr$ vs. $\Delta\log(fO_2)$ diagram; fields: 1–3, peridotite xenoliths: 1, primitive; 2, slightly metasomatized; 3, strongly metasomatized; 4, 5, abyssal peridotites with spinel (4) and plagioclase (5), after [42]; KrNrMn—lherzolite-type massifs of South Urals (Kraka, Nurali, Mindyak); Lz-Hb-766—peridotites of well 766; Lz-Hb-AZ—peridotite from Almaz-Zhemchuzhina deposit area; Hb—harzburgite, D—dunite; (d)—Diagram of PT formation conditions of mineral assemblages using pyroxene geothermometers and geobarometers [43,44]; gray points are samples of lherzolite-type massifs of South Urals.

Varied compositions of Cr-spinel indicate a clear link to mineralogical and chemical compositions of ultramafic rocks. Thus, the most high-Al spinel grains are characteristic of lherzolites ($\#Cr = 0.2\text{--}0.45$), intermediate values of Cr/Al are recorded in harzburgites ($\#Cr = 0.45\text{--}0.62$) and the most high-Cr are spinel grains from dunites ($\#Cr = 0.7\text{--}0.85$) and chromitites ($\#Cr = 0.8\text{--}0.9$). Compositions of Cr-spinel in lherzolite-harzburgite-dunite assemblages show a positive correlation between the Cr/Al and Fe/Mg ratios. However, the transition from dunites to chromitites is accompanied by a slight increase in $\#Cr$ and a significant decrease in the content of Fe (Figure 7b).

4.4. Estimates of PT - fO_2 Formation Conditions of Mineral Assemblages

To determine formation conditions of primary mineral assemblages of ultramafic rocks, we used several versions of olivine–spinel [42,45–47] and two-pyroxene geothermometers [43,44,48,49], oxygen barometer from [42] and geobarometers from [44].

It is well known that systematic discrepancies exist between the two mentioned types of geothermometers, which are generally considered as the result of different rates of equilibrium in olivine–spinel and orthopyroxene–clinopyroxene pairs (e.g., [50]). Some researchers believe that it allows us to reconstruct the history of rock cooling, on the one hand, and roughly estimate initial and final conditions of high-temperature processes stopping in the respective area of the upper mantle (e.g., [51]).

The estimates we obtained indicate that equilibrium temperatures in the Ol–Spl and Opx–Cpx pairs differ by 150–250 °C on average, and in both cases reflect temperatures of subsolidus reactions. Temperatures estimated according to the program after [44] fall in the range of 850–1150 °C. Combined with the pressure calculation, they indicate the formation of ultramafic rocks at the level of the upper mantle depths from garnet to plagioclase facies (Figure 7c). At the same time, there are two clusters that correspond to the depth ranges of 40–70 km and 15–30 km, respectively.

The assessment of redox conditions for the formation of olivine–Cr–spinel assemblages demonstrates a fairly wide range of values, from -2 to $+2.7 \Delta \log \text{FMQ} (fO_2)$, with the largest range of values typical of lherzolites. The lowest values of oxygen fugacity were found in fresh lherzolites from borehole 766, while zero and positive values prevail in host rocks of the Almaz–Zhemchuzhina deposit. In general, most of the values are comparable with the field of abyssal peridotites, as well as with those we obtained earlier for the rocks of the lherzolite massifs of the Southern Urals (Kraka, Nurali, Mindyak), ranging from -1 to $+1.5 \Delta \log \text{FMQ} (fO_2)$ (Figure 7d).

4.5. Textural Features of Olivine and Orthopyroxene According to EBSD Data

Undulose extinction of olivine and orthopyroxene grains is attributed to the distortion of the crystalline lattice as a result of plastic deformation and to the presence of low-angle grain boundaries—LABG (or subgrain boundaries) in case of recovery. Optical microscopy shows that the nature of LABG can be different, i.e., in some cases, formation of a series of parallel elongated crystal blocks (subgrain walls) is recorded, in other cases, LABGs separate approximately equiaxial areas (chessboard-type subgrains) [52]. Both types of boundaries are widespread in serpentinized ultramafic rocks of the MOF and in fresh lherzolites from borehole 766.

We studied the latter using EBSD and obtained data on the lattice preferred orientation (LPO) of olivine and orthopyroxene (Figure 8). The fabric of both minerals indicates that the rocks are mantle tectonites that were subject to high-temperature deformation in the dislocation creep regime accompanied by syntectonic recrystallization. At the same time, various types of fabric were established in the studied samples. In sample 7087, the [001] axis coincides with the lineation (L) of olivine, and the other two form girdles perpendicular to the foliation (S). This pattern is transitional between B and C fabric types of olivine and is characteristic of “wet” conditions of plastic deformation [53]. In orthopyroxene, the [001] axis also coincides with the lineation, and the (010) plane coincides with the foliation plane, which is typical of the BC type fabric of orthopyroxene [53].

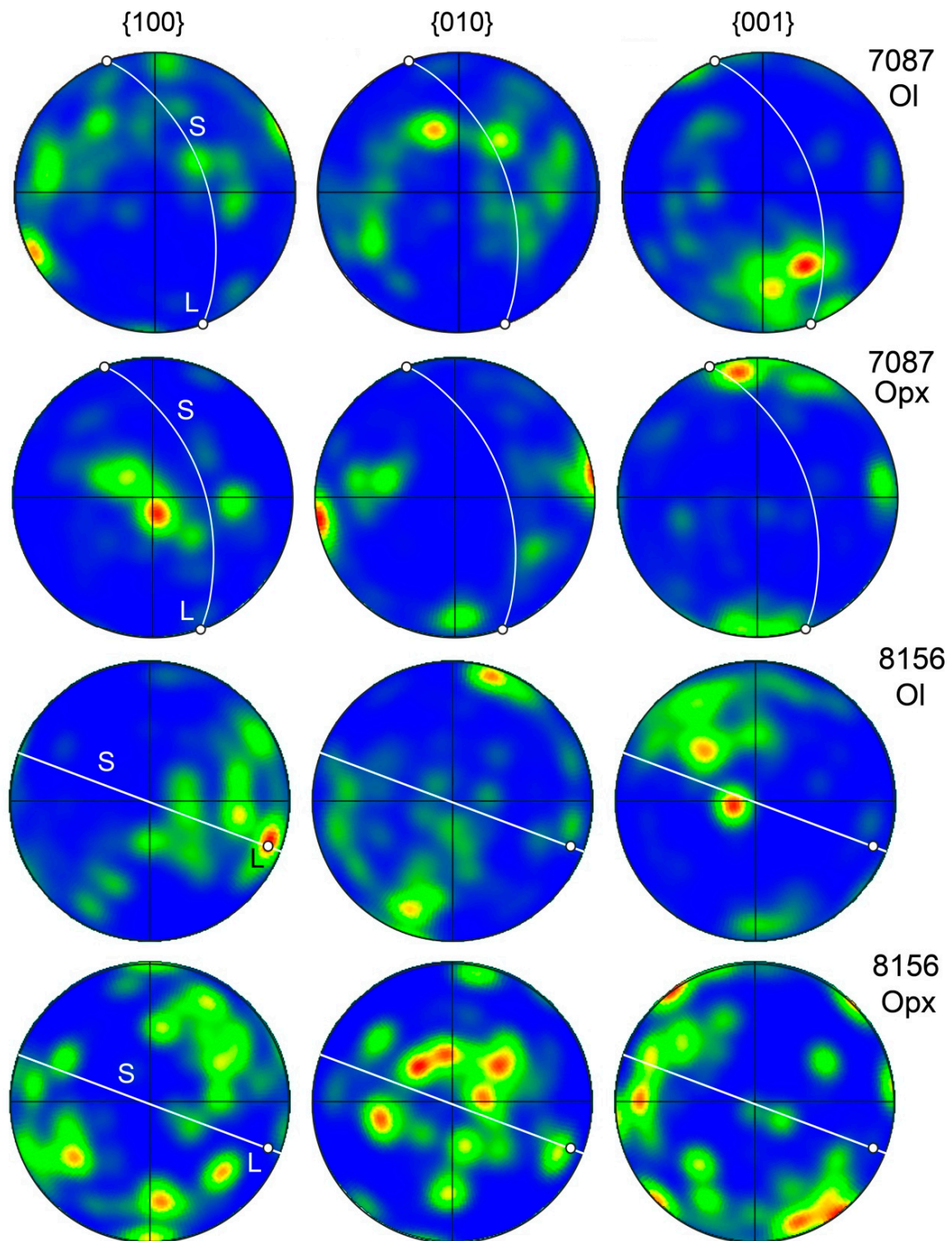


Figure 8. Olivine and orthopyroxene fabric in fresh lherzolites from well 766 of Kempirsay massif. Pole figures of the crystallographic orientation of olivine (Ol) and orthopyroxene (Opx) are presented in the upper hemisphere using an equal area projection. The color coding refers to the density of data points. S—foliation, L—lineation.

In sample 8156, the maximum of the [100] olivine axis is close to lineation, the [010] axis form the maximum almost perpendicular to the foliation, and the [001] axis is either bunched near it or inclined at an acute angle to foliation. A similar pattern is characteristic

of fabric type A [35,53], which is usually formed during slip by [100] (010) system. The axes of orthopyroxene from sample 8156 produce numerous dispersed maxima on the pole figure, which makes unambiguous interpretation difficult. The observed fabric pattern is closest to the ABC type, which was established in some experiments on the deformation of orthopyroxene [54].

4.6. Mineral Inclusions in Olivine and Orthopyroxene

Fine segregations of other phases, i.e., diopside, pargasite and Cr-spinel, with their size ranging from fractions of a micrometer to a few tens of micrometers are observed in almost all of the studied ultramafic rock samples with well-preserved relics of primary silicates, in plastically deformed orthopyroxene grains (Figures 9 and 10). They usually occur in parallel swarms in large porphyroclasts (Figure 9a,b). In the rim of large Opx grains, fine segregations of pargasite, spinel and diopside are associated with fine equiaxial olivine and enstatite grains depleted in minor elements. Inside the deformed olivine grains, there are usually rod-like or vermicular segregations of Cr-spinel and tiny segregations of pargasite (Figure 9c,d).

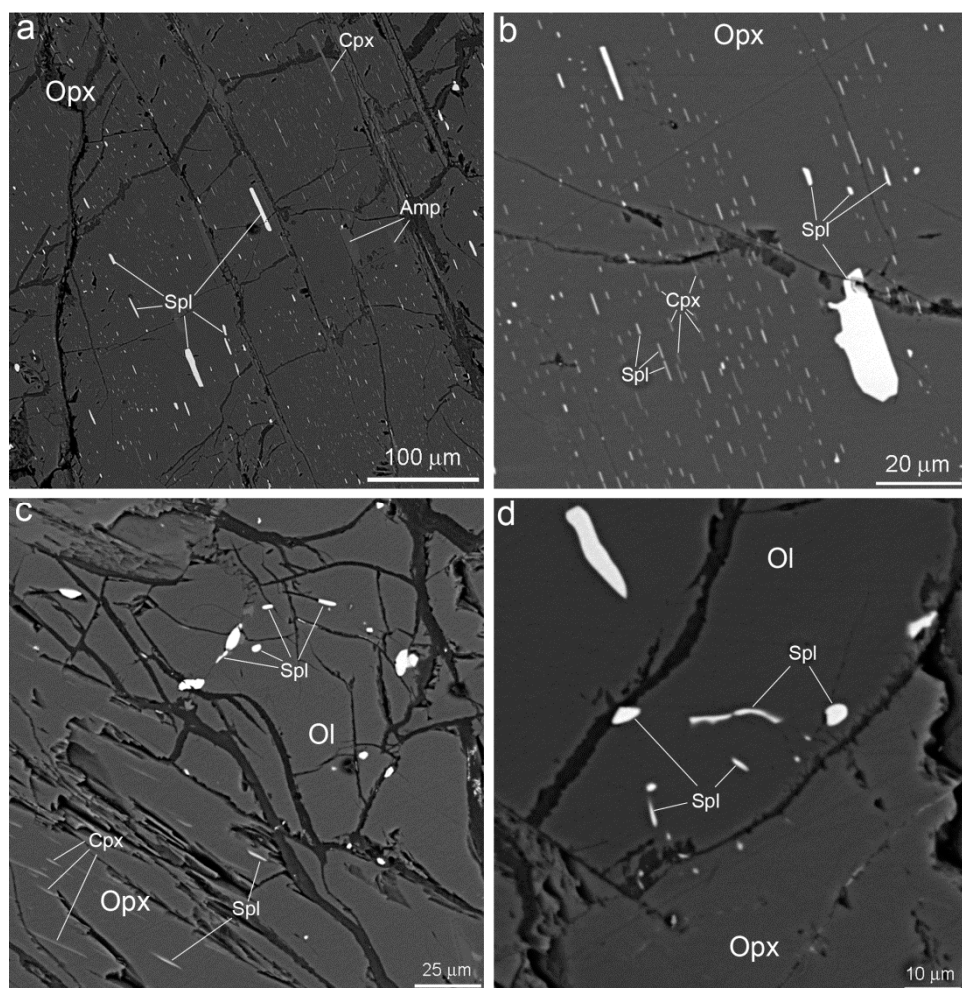


Figure 9. Cr-spinel tiny precipitates in olivine and enstatite grains: (a)—Opx porphyroclast with numerous diopside, pargasite and spinel lamellae; (b)—Detailed images of the grain: we can see growing holly-leaf Cr-spinel grain oriented parallel to lamellae; (c)—Tiny spinel precipitates in olivine grain, as well as spinel and diopside lamellae in adjacent enstatite grain; (d)—Tiny spinel precipitates in olivine grain close to boundary with enstatite grain, as well as larger spinel precipitates in olivine at a distance. All images—sample 820/300.

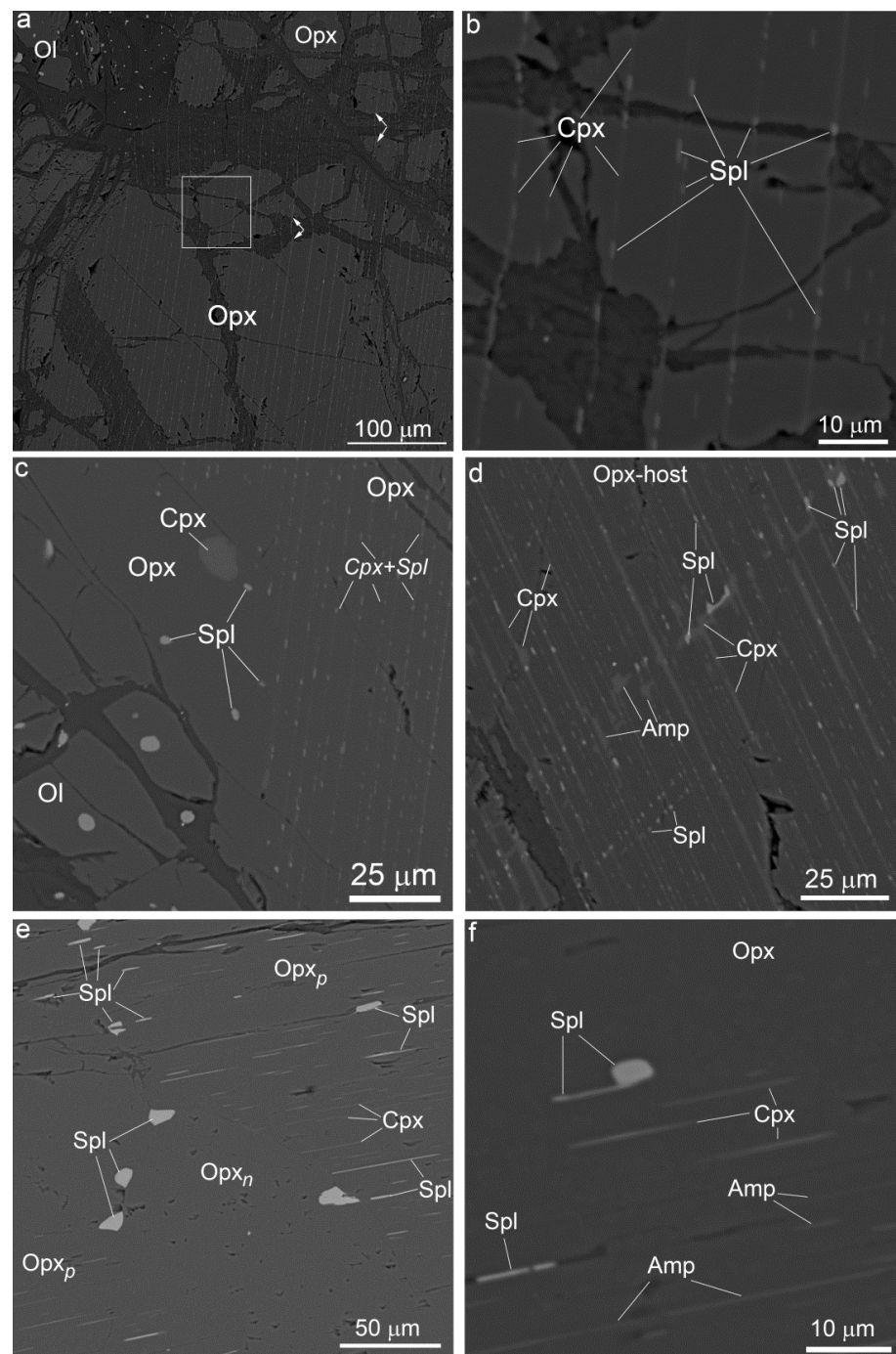


Figure 10. Formation and coalescence of precipitates in deformed orthopyroxene grain: (a)—General view of orthopyroxene porphyroclast with parallel zones containing by tiny crystals of diopside, spinel and pargasite (arrows noted bends induced by plastic deformation); (b)—Detail of the same grain (a,c)—Boundary in Opx grain: on the right, grain have fibrous structure caused by numerous sub-micrometer precipitates of spl and cpx; on the left, grain contains rare isometric inclusions of cpx and spl, similar spinel inclusions are observed in adjacent olivine grain; (d)—Detail of structure of “fibrous” Opx with numerous precipitates of pargasite, diopside and spinel; (e)—Enstatite neoblast (Opx_n) in deformed porphyroclast of the same mineral (Opx_p): in Opx porphyroclast, we can see abundant spinel and diopside lamellae but Opx neoblast associate with larger isometric grains of the same minerals; (f) –Detail of internal building of Opx porphyroclast: moment was fixed when spinel lamella are re-organizing into isometric grain. Images (a–d)—sample 809/347, (e–f)—sample 820/300.

In some cases, there is a regular change in the morphology and size of segregations with a change in the host mineral structure and the distribution style of inclusions. In particular, while abundant parallel lamellae of diopside, pargasite and spinel prevail in the central parts of large deformed orthopyroxene grains (Figure 10a,b), rare equiaxial inclusions of the diopside, pargasite and spinel with no inclusions around them are observed in the rims of the same grains (Figure 10c,e). In some cases, we observed branches from those precipitates that were equally oriented regarding lamellae in the main crystal volume (Figure 10d–f).

5. Discussion

5.1. Geodynamic Interpretation of Ultramafic Rocks

As noted above, rocks of the lherzolite-harzburgite unit predominate in the mantle section of the Kempirsay massif, while dunites and chromitites are subordinate. This set of rocks is typical of ophiolite assemblages, which are believed to have been formed by the complex action of several mantle processes, i.e., partial melting, ascending plastic flow of restite, percolation of melts (fluids) interacting with mantle peridotites (e.g., [1,19,55]).

The degree of mantle source melting is usually estimated from the compositions of accessory spinels preserved in restite [56]. The most commonly used tool for these purposes is the OSMA diagram, which presents the compositions of coexisting chrome spinel and olivine grains [57] and experimental data on the relationship between the composition of these minerals and the degree of melting of the mantle source [40]. The lherzolites and harzburgites that we studied show significantly varied compositions of Cr-spinel grains ($\#Cr = 0.2\text{--}0.65$) associated with olivine $Fo_{91\text{--}94}$. In dunites and chromitites, $\#Cr$ increases to $0.8\text{--}0.9$, and the Mg content of olivine reaches $Fo_{95\text{--}96}$. Thus, given that the varied compositions of these minerals are only attributed to the process of partial melting, the degree was proven to range from $10\%\text{--}20\%$ to 40% or more.

However, the perspective of reaching a melting degree of more than 40% is disputed by various researchers, since it is impossible to achieve the required temperatures in the upper mantle [21]. This was the reason why a different mechanism was proposed for the dunites and chromitites genesis, i.e., the reaction of restite with percolating melts (e.g., [1,58]), which was later supported by most researchers (e.g., [3,25,59–61]). A similar mechanism for the formation of the lherzolite-harzburgite-dunite association of the Kempirsay massif was substantiated in [25,27].

Estimates of the PT conditions indicate subsolidus temperatures of closure of exchange reactions in the olivine-spinel and orthopyroxene-clinopyroxene pairs. The calculated pressures suggest the subsequent formation of the section at stability levels from the top of garnet facies to the stability level of plagioclase facies. This can be interpreted as PT marks of different depth levels preserved in the rocks during the ascending rise of the mantle diapir in the plastic flow regime.

Evaluation of the redox conditions based on the composition of the olivine–spinel pairs allows us to conclude that there were predominantly reducing conditions during the formation of lherzolites from deep levels in the central part of the massif and somewhat more oxidized conditions during the formation of ore-bearing ultramafic rocks of the MOF. Similar conclusions were previously drawn for many chromite-bearing ophiolite sections of the world. However, the interpretation of the obtained results is different. In most cases, the authors make a conclusion about the suprasubduction conditions for the formation of dunites and chromitites, linking their genesis with the oxidizing conditions of the interaction of restites and boninite melts [62–64]. At the same time, high fO_2 values in the Rai-Iz dunites allowed authors of work [65] to conclude that the entire chromite-bearing section was formed in crustal conditions.

5.2. Relationship between Partial Melting, Plastic Flow, Melt-Restite Interactions as Derived from the Structure and Composition of Ultramafic Rocks

As shown above, the interpretation of only geochemical data with no microstructure of ultramafic rocks considered can lead to mutually opposite conclusions. We tried to derive the relationship between various upper mantle processes based on the comprehensive analysis of the chemical composition and microstructural features of ultramafic rock minerals.

Partial melting is reflected mainly in the variation in the composition of rock-forming silicates and Cr-spinel. With depletion from lherzolites to dunites, the Fo of olivine, and the #Cr of spinel increase in restite. However, the main problem is related to the impossibility of explaining the formation of dunites with the found compositions of coexisting olivine and Cr-spinel in this process.

The plastic flow inside the mantle diapir is imprinted in the structures of rock-forming minerals (kink bands, grain bends, undulose extinction), in the formation of the LPO of olivine and orthopyroxene. The scale of manifestation of this process in rocks is ubiquitous. In the compositions of minerals, the process of plastic flow and associated syntectonic recrystallization is indirectly reflected in the fact that enstatite neoblasts are depleted in minor and trace elements compared to large porphyroclasts of the same mineral.

The reaction of restite with percolating melts is postulated in most works on mantle sections of ophiolite complexes of the world (e.g., [4,66,67]). However, no direct evidence of this process imprinted in structures of ultramafic rocks is usually given. The proof is commonly provided by contradiction, based solely on the grounds that “dunites cannot be simple restites” [21]. This means that additional sources and/or mechanisms are needed, which can be percolating melts (interaction restite + melt). However, this does not mean that the indicated sources (mechanisms) have no alternative. In the next section, we will discuss an alternative way of dunite and Cr-spinel formation based on structural, mineralogical and geochemical facts obtained in the study of ultramafic rocks of the Kempirsay massif.

5.3. On the Cr-Spinel Source for Deposits

As noted above, the formation of dunites at the site of the original lherzolite of the upper mantle by simple partial melting is considered impossible due to a number of reasons [21]. However, this does not mean that their formation cannot be caused by partial melting as one of the main reasons (e.g., [68,69]). The second important factor for the localization of dunite bodies in the restite complex could be a large-scale plastic flow within the rising mantle diapir (e.g., [55,70]).

In previous works, we substantiated the possibility of dunite formation in the upper mantle zones of plastic deformation due to the significant difference in rheological properties of olivine and pyroxenes [12] based on numerous petrographic observations [10,23] and experimental data (e.g., [71]). Briefly, pyroxenes are unstable phases in zones of intense plastic flow that undergo progressive structural refinement, while olivine is a “weak phase”, which is more capable of grain growth during syntectonic recrystallization (e.g., [72]). This is how dunite bodies (“pathways”) appear, playing the role of “quasi-faults”, along which the mantle material rises in decompression zones.

In the fertile mantle lherzolite, chromium and aluminum are clustered in primary spinel grains, as well as in pyroxenes as minor elements and in olivine as trace elements. Assume that the fertile lherzolite has the following hypothetical composition: Ol 72% (100 ppm Al, 100 ppm Cr), Opx 20% (4 wt.% Al, 1 wt.% Cr), Cpx 7% (4 wt.% Al, 1.5 wt.% Cr), Spl 1% (25 wt.% Al, 25 wt.% Cr). Then the chromium balance can be represented by the following values (wt.%): $Spl = 0.01 \times 25 = 0.25$; $Opx = 0.2 \times 1 = 0.2$; $Cpx = 0.07 \times 1.5 = 0.11$; $Ol = 0.72 \times 0.01 = 0.007$. Thus, in case of the complete decomposition of pyroxenes, a comparable amount of new grains of Cr-spinels, about 2%, should be formed in the volume of rock composed only of olivine.

Similar data are also provided by supporters of the reaction formation of Cr-spinels during the dissolution of pyroxenes and crystallization of olivine (e.g., [21]). However, the

mechanism of further concentration of newly formed grains of Cr-spinel remains beyond consideration, since it does not logically follow from the hypothesis itself. In the case of the deformation-induced decomposition of pyroxenes [10,23], the same mechanism continues to operate, namely, the plastic flow of restite. During this, phases with contrast physical properties, chromite, and olivine, should be segregated and, thus, chromitite ore bodies are formed. In previous works, we carried out simulation data that allowed us to thermodynamically substantiate the segregation of phases with different properties in a two-phase plastic flow (dunite) [12].

The studied samples of lherzolites and harzburgites of the Kempirsay massif show numerous examples of deformation-induced decomposition of pyroxenes, as illustrated in Figures 9 and 10. Noteworthy, enstatite-II, forsterite, pargasite and diopside are complementary phases of pyroxene decomposition and Cr-spinel formation. Enstatite neoblasts are extremely depleted in impurities. The first two minerals remain in restite, but the latter two must turn into a partial melt due to the low melting point. Thus, the whole process involves the simultaneous action of two main mechanisms, i.e., the plastic flow of mantle peridotite and its partial melting, which can be mutually initiated.

5.4. Chromitite Formation Model

To sum up, we propose the following sequence of chromitite deposits formation in the Kempirsay massif. The initial stage of dunite bodies separation and the early accumulation of additional Cr-spinel grains in them is associated with the start of the mantle upwelling under rift conditions (decompression rise). On the grain scale, the rise was reflected in the dislocation creep, including the glide and syntectonic recrystallization of rock-forming minerals, i.e., olivine and orthopyroxene.

The most efficient glide occurred in olivine, since many slip systems can be activated in this mineral and thus it is the “weakest” upper mantle material (e.g., [10,11,71,72]). On the contrary, orthopyroxene underwent “deformation-induced decomposition” with the formation of new phases: Cr-spinel, forsterite, pargasite and diopside [10]. The former two minerals remained in the restite, while the latter were removed along with the partial melt (Figure 11a). Thereby, in areas where this process was the most intense, the plastic flow should have allocated the result of an increased concentration of the weaker phase, olivine, and fluid (partial melt). Notably, the described mechanism of the mutual action of plastic flow and partial melting requires no external sources, which is typical of “reaction models”.

It should also be noted that, in terms of petrography, the “melt” as xenomorphic diopside and pargasite grains is fixed only at the initial stage of dunite formation and in very small quantities. In the vast majority of cases, chromite-bearing dunites show no signs of active percolation of melts. This suggests that the separation of the liquid phase from dunites occurred at the earliest stages of the process and then the melts migrated mainly without connection with the zones of localized plastic flow.

We can assume various scenarios for the mantle diapir rise with two extreme cases, i.e., an increased number of small “flow/melt” zones or expanded scales of one or several zones. Both options are geologically validated by successive alternation of dunite-harzburgite (thickness from a few cm to a few meters) in the first case and by large bodies of dunites hundreds of meters thick among peridotites in the second case, e.g., [11]. In addition, as the diapir moves towards the surface, the initial stage may appear in new areas, while in others, already advanced stages of the process will take place.

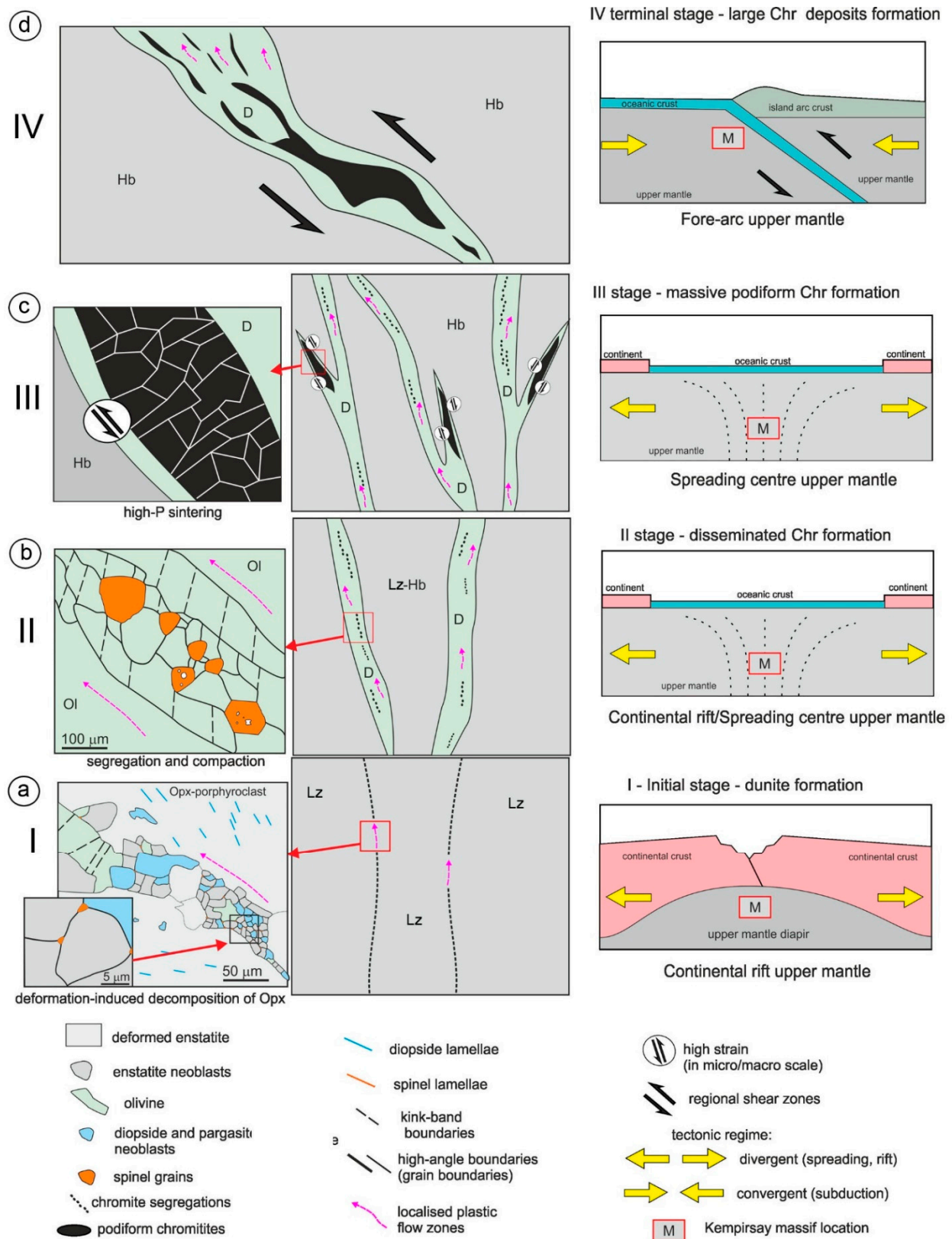


Figure 11. General model of Kempirsay chromitite deposits formation: (a)—initial stage of dunite formation, (b)—stage of disseminated chromitite formation, (c)—stage of massive podiform chromitite formation, (d)—terminal stage of large chromitite deposits formation.

At the next stage, when dunite with an increased number of Cr-spinel grains (2%–5%) is already isolated, a more intense flow inside it leads to effective segregation of phases with contrasting physical properties (olivine-chromite), which mechanism is studied in detail in [12]. This is how the bodies of disseminated chromitites are formed (Figure 11b). The solid-state flow origin of these ores is clearly traced in the round shape of the chromite grains and in tectonite textures of olivine from interstices of these grains [73].

The transition from disseminated to massive textures of ores can be considered an advanced stage of the chromitite formation (Figure 11c). This is a logical continuation of the process of the olivine and chromite segregation in the dunite body. However, such a transition would have important dynamic and geological implications. As long as each fine chromite grain was enclosed in a weak olivine matrix, the entire dunite body could continue to be a zone of localized deformation. However, with the impingement of grains and consequent coarsening of grains/aggregates of chromite, rheological properties of dunite in general should change. Chromite-free areas continue to accommodate strain through plastic flow, but strain will accumulate in ore areas, which can provide local heating and increased pressure. As a result, there will be the “pressure sintering” effect inside ore areas, on the one hand, and special separation of ore and barren areas inside dunite, on the other hand (Figure 11c).

Geological observations fairly witness the above assumption: (1) disseminated ores are usually composed of fine grains (<1 mm) and occur inside large dunite bodies in the form of numerous flattened discontinuous deposits with the banded texture, (2) massive ores are composed of medium- to coarse-grained chromitites with stressed textures and usually separated from harzburgites by thin dunite envelopes, (3) nodular ores are most often found close to the rim of massive chromitites and have signs of the tectonic origin [74,75].

All the above stages of the chromitite formation can be implemented in a single mode of upper mantle uplift. There is no need to involve numerous external sources, melts, and fluids with varied compositions to explain the stages. Notably, the leading role of deformation processes in formation of massive Vourinos chromitites has been recently deduced based on structural criteria in [13]. As for the mineral microinclusions in chromite grains, they could be captured in different ways both at early stages of dunite separation [76] and as a result of annealing recrystallization that accompanied the “pressure sintering” process during the formation of massive chromitites.

However, a concurrence of favorable conditions (final stage) is necessary for the formation of unique chromite deposits, which are not single pods or lenses, as in most ophiolite massifs, but complex deposits consisting of several intergrown bodies, like in the MOF of the Kempirsay. As a possible factor, we can indicate a change in the geodynamic regime in the upper mantle of the region, which was superimposed on numerous single podiform bodies formed here during rifting (Figure 11d). The geological and geochemical data indicate fore-arc settings of the Kempirsay ultramafic rocks formation [25]. It is therefore logical to assume that this area of the mantle with numerous minor chromitite bodies was subject to shear with compression under PT mantle conditions. As a result, these bodies in the dunite envelopes were brought together to form the largest deposits localized in the center of “ore bunches”, diverging towards the surface.

6. Conclusions

Geological, structural, petrographic, and mineralogical evidence indicates that rock-forming minerals of non-depleted lherzolites from the upper mantle of source region are the source for the unique chromium deposits in the south-eastern part of the Kempirsay massif. Plastic flow and partial melting were key processes that provided redistribution of chromium from silicate mantle minerals to the deposits. Their combined manifestation was caused by a decompression rise of the mantle diapir at the divergent regime of the Uralian belt (basin) evolution.

The sequence of formation of chromitites is as follows: (1) formation of new Cr-spinel grains in result of deformation-induced decomposition of orthopyroxenes, (2) formation of

dunite zones of plastic flow in restite, wherein Cr-spinel grains accumulate and segregate, (3) formation of disseminated grains as a result of segregation in the plastic flow of dunite, (4) formation of massive chromitites by pressure sintering. Formation of unique chromitite deposits is associated with integration of numerous disparate podiform bodies into “ore bunches” due to tectonic action in the shear-compression regime. The latter was most likely associated with the transition of the divergent regime (rift, spreading) to that of the upper mantle in the fore-arc basin.

Although we have constructed a complete and consistent model for the chromitites formation in the Kempirsay massif, some particular issues remain unsolved. The key problem is the evolution of the chemical composition of Cr-spinel in the ore-forming process and the origin of the varied composition of ore-forming spinels at different deposits.

Author Contributions: Conceptualization, D.E.S. and D.K.M.; methodology, D.E.S. and V.V.S.; software, D.E.S., I.R.R. and R.A.G.; validation, D.E.S., D.K.M. and I.R.R.; formal analysis, D.E.S.; investigation, D.E.S.; resources, D.E.S., D.K.M. and R.A.G.; data curation, D.E.S. and D.K.M.; writing—original draft preparation, D.E.S. and I.R.R.; writing—review and editing, D.E.S., D.K.M. and I.R.R.; visualization, D.E.S. and R.A.G.; supervision, D.E.S., D.K.M. and I.R.R.; funding acquisition, D.E.S. and I.R.R. All authors have read and agreed to the published version of the manuscript.

Funding: This study was supported by the Russian Science Foundation grant No. 22-17-00019 (<https://rscf.ru/project/22-17-00019/>) (accessed on 11 May 2022). Analytical studies were carried out using the equipment of the resource centers “Geomodel” and “Nanophotonics” of the Science Park of St. Petersburg State University. Field works were performed as part of government contract no. FMRS–2022–0011.

Data Availability Statement: The data presented in this study are available on request from the corresponding author.

Acknowledgments: The authors are very grateful to our colleagues from “ERG Exploration” Shalabayev Azamat Zhenisovich, Ichenko Andrey Mikhailovich, Khamzin Aydar Berikbolovich, Makatov Dastan Kayratovich, Ulukpanov Kuandyk Taskinbaevich, Alimov Sultan for very useful field trip on the Main Ore field deposits and Chaschukin Igor Stepanovich and Chernyshov Alexey Ivanovich for providing samples of cores from deep bore holes of Kempirsay massif. We are also very grateful to two anonymous reviewers for useful comments that allowed us to significantly improve the manuscript.

Conflicts of Interest: The authors declare no conflict of interest.

References

1. Kelemen, P. Reaction between ultramafic rock and fractionating basaltic magma I. Phase relations, the origin of calc-alkaline magma series, and the formation of discordant dunite. *J. Petrol.* **1990**, *31*, 51–98. [[CrossRef](#)]
2. Arai, S. Origin of podiform chromitites. *J. Asian Earth Sci.* **1997**, *15*, 303–310. [[CrossRef](#)]
3. Nayak, R.; Pal, D.; Chinnasamy, S.S. High-Cr chromitites of the Nidar Ophiolite Complex, northern India: Petrogenesis and tectonic implications. *Ore Geol. Rev.* **2021**, *129*, 103942. [[CrossRef](#)]
4. Morishita, T.; Andal, E.S.; Arai, S.; Ishida, Y. Podiform chromitites in the lherzolite-dominant mantle section of the Isabela ophiolite, the Philippines. *Isl. Arc* **2006**, *15*, 84–101. [[CrossRef](#)]
5. Farré-de-Pablo, J.; Pujol-Solà, N.; Torres-Herrera, H.; Aiglsperger, T.; González-Jiménez, J.M.; Llanes-Castro, A.I.; Garcia-Casco, A.; Proenza, J.A. Orthopyroxenite hosted chromitite veins anomalously enriched in platinum-group minerals from the Havana-Matanzas Ophiolite, Cuba. *Boletín De La Soc. Geológica Mex.* **2020**, *72*, A110620. [[CrossRef](#)]
6. Borisova, A.Y.; Ceuleneer, G.; Kamenetsky, V.S.; Arai, S.; Bějina, F.; Abily, B.; Bindeman, I.N.; Polvé, M.; De Parseval, P.; Aigouy, T.; et al. A new view on the petrogenesis of the Oman ophiolite chromitites from microanalyses of chromite-hosted inclusions. *J. Petrol.* **2012**, *53*, 2411–2440. [[CrossRef](#)]
7. Pushkarev, E.V.; Kamenetsky, V.S.; Morozova, A.V.; Khiller, V.V.; Glavatskykh, S.P.; Rodemann, T. Ontogeny of ore Cr-spinel and composition of inclusions as indicators of the pneumatolytic-hydrothermal origin of PGM-bearing chromitites from Kondyor massif, the Aldan Shield. *Geol. Ore Depos.* **2015**, *57*, 352–380. [[CrossRef](#)]
8. Arai, S.; Akizawa, N. Precipitation and dissolution of chromite by hydrothermal solutions in the Oman ophiolite: New behavior of Cr and chromite. *Am. Miner.* **2014**, *99*, 28–34. [[CrossRef](#)]
9. Arai, S.; Miura, M.; Tamura, A.; Arizawa, N.; Ishikawa, A. Hydrothermal Chromitites from the Oman Ophiolite: The Role of Water in Chromitite Genesis. *Minerals* **2020**, *10*, 217. [[CrossRef](#)]

10. Saveliev, D.E.; Puchkov, V.N.; Sergeev, S.N.; Musabirov, I.I. Deformation-induced decomposition of enstatite in mantle peridotite and its role in partial melting and chromite ore formation. *Dokl. Earth Sci.* **2017**, *476*, 1058–1061. [[CrossRef](#)]
11. Saveliev, D.E. Chromitites of the Kraka ophiolite (South Urals, Russia): Geological, mineralogical and structural features. *Miner. Depos.* **2021**, *56*, 1111–1132. [[CrossRef](#)]
12. Saveliev, D.E.; Fedoseev, V.B. Solid-state redistribution of mineral particles in the upwelling mantle flow as a mechanism of chromite concentration in the ophiolite ultramafic rocks (by the example of Kraka ophiolite, the Southern Urals). *Georesources* **2019**, *21*, 31–46. [[CrossRef](#)]
13. Rassios, A.; Tzamos, E.; Dilek, Y.; Bussolesi, M.; Grieco, G.; Batsi, A.; Gamaletsos, P.N. A structural approach to the genesis of chrome ores within the Vourinos ophiolite (Greece): Significance of ductile and brittle deformation processes in the formation of economic ore bodies in oceanic upper mantle peridotites. *Ore Geol. Rev.* **2020**, *125*, 103684. [[CrossRef](#)]
14. Kravchenko, G.G. *The Role of Tectonics in the Crystallization of Chromite Ores of the Kempirsay Pluton*; Nauka: Moscow, Russia, 1969; 232p. (In Russian)
15. Pavlov, N.V.; Kravchenko, G.G.; Chuprykina, I.I. *Chromites of Kempirsay Pluton*; Nauka: Moscow, Russia, 1968; 178p. (In Russian)
16. Chaschukhin, I.S.; Votyakov, S.L.; Schapova, Y.V. *Crystal Chemistry of Cr-Spinel and Oxythermobarometry of Ultramafic Rocks of Folded Regions*; IGG UB RAS: Ekaterinburg, Russia, 2007; 310p. (In Russian)
17. Johnson, C. Podiform Chromite at Voskhod, Kazakhstan. Ph.D. Thesis, Cardiff University, Cardiff, UK, 2012; 468p. Available online: <https://orca.cardiff.ac.uk/id/eprint/40714> (accessed on 1 May 2022).
18. Sokolov, G.A. *Chromitites of Urals, Their Composition, Crystallization Conditions and Regularities of Distribution*; Trudy of IGN AN USSR: Moscow, Russia, 1948; Volume 97, 128p. (In Russian)
19. Ringwood, A.E. *Composition and Structure of the Earth's Mantle*; McGraw-Hill: New York, NY, USA.; London, UK; Sydney, NSW, Australia, 1975; 618p.
20. Anderson, D.L. *Theory of the Earth*; Blackwell Scientific Publication: Boston, MA, USA, 1989; 366p.
21. Kelemen, P.B.; Shimizu, N.; Salters, V. Extraction of mid-ocean-ridge basalt from the upwelling mantle by focused flow of melt in dunite channels. *Nature* **1995**, *375*, 747–753. [[CrossRef](#)]
22. Ballhaus, C. Origin of the podiform chromite deposits by magma mingling. *Earth Planet. Sci. Lett.* **1998**, *156*, 185–193. [[CrossRef](#)]
23. Saveliev, D.E.; Shilovskikh, V.V.; Sergeev, S.N.; Kutyrev, A.V. Chromian spinel neomineralisations and the microstructure of plastically deformed ophiolitic peridotites (Kraka massifs, Southern Urals, Russia). *Miner. Petrol.* **2021**, *115*, 411–430. [[CrossRef](#)]
24. Savelieva, G.N.; Pertsev, A.N. Mantle ultramafic rocks in ophiolites of Kempirsay massif. *Petrologiya* **1995**, *3*, 115–132. (In Russian)
25. Melcher, F.; Grum, W.; Simon, G.; Thalhammer, T.V.; Stumpfl, E.F. Petrogenesis of the ophiolitic giant chromite deposits of Kempirsai, Kazakhstan: A study of solid and fluid inclusions in chromite. *J. Petrol.* **1997**, *38*, 1419–1458. [[CrossRef](#)]
26. Chashchukhin, I.S.; Votyakov, S.L. Behavior of iron-group elements, oxybarometry, and genesis of unique chromite deposits in the Kempirsai massif. *Geol. Ore Depos.* **2009**, *51*, 123–138. [[CrossRef](#)]
27. Melcher, F.; Grum, W.; Thalhammer, T.; Thalhammer, O.A.R. The giant chromite deposits at Kempirsai, Urals: Constraints from trace element (PGE, REE) and isotope data. *Mineral. Deposita* **1999**, *34*, 250–272. [[CrossRef](#)]
28. Melcher, F. Base metal—Platinum-group element sulfides from the Urals and the Eastern Alps: Characterization and significance for mineral systematics. *Mineral. Petrol.* **2000**, *68*, 177–211. [[CrossRef](#)]
29. Distler, V.; Kryachko, V.; Yudovskaya, M. Ore petrology of chromite-PGE mineralization in the Kempirsai ophiolite complex. *Mineral. Petrol.* **2008**, *92*, 31–58. [[CrossRef](#)]
30. Abdullin, A.A.; Avdeev, A.V.; Seitov, N.S. *Ophiolites of Sakmara and Or-Ilez Zones of Mugodzhars*; Works of Institute of Geological Sciences of KazSSR, Nauka: Alma-Ata, Kazakhstan, 1975; pp. 39–74. (In Russian)
31. Saveliev, A.A.; Savelieva, G.N. Ophiolites of the Kempirsay massif: Main features of structural and material evolution. *Geotectonika* **1991**, *6*, 57–75. (In Russian)
32. Puchkov, V.N. Structure and geodynamics of the Uralian orogen. In *Orogeny Through Time*; Geological Society. Special Publications: London, UK, 1997; Volume 121, pp. 201–236. [[CrossRef](#)]
33. Kolotilov, L.I.; Kazantsev, M.M.; Razbaum, E.I. *Structural and Morphological Zoning of Ore Clusters in the South Kempirsai Chromite Region, Its Prospecting and Estimated Value*; Geology, Metallogeny and Material Composition of Ferrous Metal Ores: Alma-Ata, Kazakhstan, 1979; pp. 64–70. (In Russian)
34. Gorelik, S.S. *Recrystallization of Metals and Alloys*; Metallurgiya: Moscow, Russia, 1978. (In Russian)
35. Karato, S.-I. *Deformation of Earth Materials. An Introduction to the Rheology of Solid Earth*; Cambridge University Press: Cambridge, UK, 2008; 463p. [[CrossRef](#)]
36. Mercier, J.C.; Nicolas, A. Textures and fabrics of upper mantle peridotites as illustrated by basalt xenoliths. *J. Petrol.* **1975**, *16*, 454–487. [[CrossRef](#)]
37. Leblanc, M. Chromite growth, dissolution and deformation from a morphological view point: SEM investigations. *Miner. Depos.* **1980**, *15*, 201–210. [[CrossRef](#)]
38. Matsumoto, I.; Arai, S. Morphological and chemical variations of chromian spinel in dunite-harzburgite complexes from the Sangun zone (SW Japan): Implications for mantle/melt reaction and chromite formation processes. *Mineral. Petrol.* **2001**, *73*, 305–323. [[CrossRef](#)]
39. Thayer, T.P. Principal features and origin of podiform chromite deposits, and some observation on the Guleman-Soridag district, Turkey. *Econ. Geol.* **1964**, *59*, 1497–1524. [[CrossRef](#)]

40. Jaques, A.L.; Green, D.H. Anhydrous melting of peridotite at 0–15 kb pressure and the genesis of tholeiitic basalts. *Contrib. Mineral. Petrol.* **1980**, *73*, 287–310. [[CrossRef](#)]
41. Saveliev, D.E.; Shilovskikh, V.V.; Makatov, D.K.; Gataullin, R.A. Accessory Cr-spinel from peridotite massifs of the South Urals: Morphology, composition and origin. *Miner. Petrol.* **2022**. under review.
42. Ballhaus, C.; Berry, R.F.; Green, D.H. High pressure experimental calibration of the olivine-orthopyroxene-spinel oxygen geobarometer: Implications for the oxidation state of the upper mantle. *Contr. Miner. Petrol.* **1991**, *107*, 27–40. [[CrossRef](#)]
43. Brey, G.P.; Köhler, T. Geothermobarometry in 4-phase lherzolites: 2. New thermobarometers, and practical assessment of existing thermobarometers. *J. Petrol.* **1990**, *31*, 1353–1378. [[CrossRef](#)]
44. Putirka, K.D. Thermometers and barometers for volcanic systems. *Rev. Mineral. Geochem.* **2008**, *69*, 61–120. [[CrossRef](#)]
45. Fabriès, J. Spinel-olivine geothermometry in peridotites from ultramafic complexes. *Contrib. Mineral. Petrol.* **1979**, *69*, 329–336. [[CrossRef](#)]
46. Roeder, P.L.; Campbell, I.H.; Jamieson, H.E. A re-evaluation of the olivine-spinel geothermometer. *Contrib. Mineral. Petrol.* **1979**, *68*, 325. [[CrossRef](#)]
47. Ono, A. Fe-Mg partitioning between spinel and olivine. *J. Jpn. Assoc. Mineral. Petrol. Econ. Geol.* **1983**, *78*, 115–122. [[CrossRef](#)]
48. Wood, B.J.; Banno, S. Garnet-orthopyroxene and orthopyroxene-clinopyroxene relationships in simple and complex systems. *Contrib. Mineral. Petrol.* **1973**, *42*, 109–124. [[CrossRef](#)]
49. Wells, P.R.A. Pyroxene thermometry in simple and complex systems. *Contrib. Mineral. Petrol.* **1977**, *62*, 129–139. [[CrossRef](#)]
50. Ozawa, K. Evaluation of olivine-spinel geothermometry as an indicator of thermal history for peridotites. *Contrib. Mineral. Petrol.* **1983**, *82*, 52–65. [[CrossRef](#)]
51. Ozawa, K.; Takahashi, N. P-T history of a mantle diapir: The Horoman peridotite complex, Hokkaido, northern Japan. *Contrib. Mineral. Petrol.* **1995**, *120*, 223–248. [[CrossRef](#)]
52. Passchier, C.W.; Trouw, R.A.J. *Microtectonics*, 2nd ed.; Revised and Enlarged Edition; Springer: Berlin/Heidelberg, Germany, 2005; 366p.
53. Jung, H. Crystal preferred orientations of olivine, orthopyroxene, serpentine, chlorite, and amphibole, and implications for seismic anisotropy in subduction zones: A review. *Geosci. J.* **2017**, *21*, 985–1011. [[CrossRef](#)]
54. Jung, H.; Park, M.; Jung, S.; Lee, J. Lattice preferred orientation, water content, and seismic anisotropy of orthopyroxene. *J. Earth Sci.* **2010**, *21*, 555–568. [[CrossRef](#)]
55. Nicolas, A.; Bouchez, J.L.; Boudier, F.; Mercier, J.-C. Textures, structures and fabrics due to solid state flow in some European lherzolites. *Tectonophysics* **1971**, *12*, 55–86. [[CrossRef](#)]
56. Dick, H.J.B.; Bullen, T. Chromian spinel as a petrogenetic indicator in abyssal and alpine-type peridotites and spatially associated lavas. *Contrib. Mineral. Petrol.* **1984**, *86*, 54–76. [[CrossRef](#)]
57. Arai, S. Characterization of spinel peridotites by olivine-spinel compositional relationships: Review and interpretation. *Chem. Geol.* **1994**, *113*, 191–204. [[CrossRef](#)]
58. Arai, S.; Yurimoto, H. Podiform chromitites from the Tari-Misaka ultramafic complex, southwestern Japan, as a melt mantle interaction products. *Econ. Geol.* **1994**, *89*, 1279–1288. [[CrossRef](#)]
59. Zhou, M.-F.; Robinson, P.T.; Malpas, J.; Li, Z. Podiform Chromitites in the Luobusa Ophiolite (Southern Tibet): Implications for Melt-Rock Interaction and Chromite Segregation in the Upper Mantle. *J. Petrol.* **1996**, *37*, 3–21. [[CrossRef](#)]
60. Payot, B.D.; Arai, S.; Tamayo, R.A.; Yumul, G.P. Textural evidence for the chromite-oversaturated character of the melt involved in podiform chromitite formation. *Resour. Geol.* **2013**, *63*, 313–319. [[CrossRef](#)]
61. Park, G.; Park, J.-W.; Heo, C.-H.; Kim, J. Distribution of mantle-melt interaction zone: A petrological exploration tool for podiform chromitite deposits in the Kalaymyo ophiolite, Myanmar. *J. Geochem. Explor.* **2022**, *232*, 106878. [[CrossRef](#)]
62. Liu, J.; Wang, J.; Hattori, K.; Wang, Z.; Zhang, H. Early Palaeozoic sub-arc chromitite-bearing peridotite in the Kudi ophiolite on the westernmost Tibetan Plateau. *Int. Geol. Rev.* **2019**, *61*, 1105–1123. [[CrossRef](#)]
63. Xiong, F.; Zoheir, B.; Robinson, P.T.; Yang, J.; Xu, X.; Meng, F. Genesis of the Ray-Iz chromitite, Polar Urals: Inferences to mantle conditions and recycling processes. *Lithos* **2020**, *374–375*, 105699. [[CrossRef](#)]
64. He, Y.; Zhu, X.; She, Y.; Ma, J.; Sun, J.; Gao, Z.; Wan, H.; Chen, Y. Mechanism of formation of podiform chromitite: Insights from the oxidation states of podiform chromitites and host peridotites from the Luobusa ophiolite, southern tibet. *Ore Geol. Rev.* **2021**, *139*, 104483. [[CrossRef](#)]
65. Shyryaev, P.B. Oxythermobarometry, Composition and Genetic Features of Chromium Ores from Rai-Iz and Voykar-Synya Ultramafic Massifs (Polar Urals). Ph.D. Thesis, IGM RAS, Moscow, Russia, 2021. (In Russian).
66. Gonzalez-Jimenez, J.M.; Griffin, W.L.; Proenza, A.; Gervilla, F.; O'Reilly, S.Y.; Akbulut, M.; Pearson, N.J.; Arai, S. Chromitites in ophiolites: How, where, when, why? Part II. The crystallization of chromitites. *Lithos* **2014**, *189*, 148–158. [[CrossRef](#)]
67. Ullah, Z.; Shah, M.T.; Siddiqui, R.H.; Lian, D.-Y.; Khan, A. Petrochemistry of High-Cr and High-Al chromitites occurrences of Dargai Complex along Indus Suture Zone, Northern Pakistan. *Episodes* **2020**, *43*, 689–709. [[CrossRef](#)]
68. Arai, S. Dunitite-harzburgite-chromitite complexes as refractory residue in the Sangun-Yamaguchi zone, western Japan. *J. Petrol.* **1980**, *21*, 141–165. [[CrossRef](#)]
69. Leblanc, M.; Nicolas, A. Ophiolitic chromitites. *Int. Geol. Rev.* **1992**, *34*, 653–686. [[CrossRef](#)]
70. Cassard, D.; Nicolas, A.; Rabinowitch, M.; Moutte, J.; Leblanc, M.; Prinzhofer, A. Structural Classification of Chromite Pods in Southern New Caledonia. *Econ. Geol.* **1981**, *76*, 805–831. [[CrossRef](#)]

71. Yamamoto, J.; Ando, J.; Kagi, H.; Inoue, T.; Yamada, A.; Yamazaki, D.; Irifune, T. In situ strength measurements on natural upper-mantle minerals. *Phys. Chem. Miner.* **2008**, *35*, 249–257. [[CrossRef](#)]
72. Carter, N.L. Steady state flow of rocks. *Rev. Geophys. Space Phys.* **1976**, *14*, 301–360. [[CrossRef](#)]
73. Saveliev, D.E.; Shilovskikh, V.V.; Sergeev, S.N. Microstructural Patterns of Ophiolitic Chromitite of the Kraka Massif, South Urals. I. Banded Disseminated Ores. *Geol. Ore Depos.* **2021**, *63*, 812–829. [[CrossRef](#)]
74. Saveliev, D.E. Origin of nodular structures (on the example eastern part of Central Kraka massif, the Southern Urals). *Rudy I Met.* **2013**, *5*, 41–49. (In Russian)
75. Zhang, P.-F.; Zhou, M.-F.; Liu, Q.-Y.; Malpas, J.; Robinson, P.T.; He, Y.-S. Modification of mantle rocks by plastic flow below spreading centers: Fe isotopic and fabric evidence from the Luobusa ophiolite, Tibet. *Geochim. Cosmochim. Acta* **2019**, *253*, 84–110. [[CrossRef](#)]
76. Saveliev, D.E.; Musabirov, I.I. About formation mechanisms of accessory Cr-spinels in plastically deformed enstatite of Kraka massifs (Uralian ophiolitic belt). *Zap. RMO* **2019**, *148*, 28–49. (In Russian) [[CrossRef](#)]